1. GAMMA-RAY DETECTORS FOR NONDESTRUCTIVE ANALYSIS

P. A. Russo and D. T. Vo

I. INTRODUCTION AND OVERVIEW

Gamma rays are used for nondestructive quantitative analysis of nuclear material. Knowledge of both the energy of the gamma ray and its rate of emission from the unknown mass of nuclear material is required to interpret most measurements of nuclear material quantities. Therefore, detection of gamma rays for nondestructive analysis of nuclear materials requires both spectroscopy capability and knowledge of absolute specific detector response.

Some techniques nondestructively quantify attributes other than nuclear material mass, but all rely on the ability to distinguish elements or isotopes and measure the relative or absolute yields of their corresponding radiation signatures. All require spectroscopy and most require high resolution. Therefore, detection of gamma rays for quantitative nondestructive analysis (NDA) of the mass or of other attributes of nuclear materials requires spectroscopy.

A previous book on gamma-ray detectors for NDA[1] provided generic descriptions of three detector categories: inorganic scintillation detectors, semiconductor detectors, and gas-filled detectors. This report described relevant detector properties, corresponding spectral characteristics, and guidelines for choosing detectors for NDA. The current report focuses on significant new advances in detector technology in these categories. Emphasis here is given to those detectors that have been developed at least to the stage of commercial prototypes. The type of NDA application – fixed installation in a count room, portable measurements, or fixed installation in a processing line or other active facility (storage, shipping/receiving, *etc.*) – influences the choice of an appropriate detector.

Some prototype gamma-ray detection techniques applied to new NDA approaches may revolutionize how nuclear materials are quantified in the future. An example is gamma-ray NDA applied to quantitative measurements of in-process nuclear materials. Such measurements are routinely performed with rugged, reliable, stable, sensitive portable detectors[2, 3] but could be accomplished with distributed networked sensors (DNS). The approach requires gamma-ray detectors that are lower in cost (because DNS uses a large number of detectors) but have the ruggedness, reliability, stability, and sensitivity of the portable detectors. Modern safeguards concepts for verifying inventory and tracking transfers and movements of nuclear materials invoke DNS approaches.[4] Sophisticated imaging detectors may eventually satisfy some needs for DNS. Prototype commercial alternatives to traditional gamma-ray detectors that apply to portable applications, DNS, and imaging are described in this report.

Low-resolution alkali halides (NaI and CsI) and bismuth germanate ($Bi_4Ge_3O_{12}$, or BGO) were available previously[5] and have been in use with photomultiplier tubes (PMTs) almost exclusively.[6] A tremendous growth in options for PMT design enhances the usefulness of such scintillators in compact scintillator/PMT detectors that give optimum performance. Semiconductor alternatives to PMTs for converting scintillation light to electronic pulses can further reduce the size of a detector package for a given scintillator and improve the overall ruggedness of the assembly. Ruggedized assemblies now allow good scintillator/PMT performance under high mechanical stress. Analog and digital approaches to gain stabilization are available commercially, and the latter is straightforward to implement with user-developed software.[7]

Families of new scintillator materials with improved characteristics are now available in large sizes. Some with higher-Z metallic species actually compete favorably with BGO for high density but also have a natural radioisotope. An example is lutetium oxyorthosilicate, $Lu_2(SiO4)O(Ce)$ or LSO, which, though slightly better in resolution than BGO, is impractical for many if not most applications because of its relatively high intrinsic radiation.[8, 9] The density range of two cerium-doped lanthanum

halides varies from ~1.1 times that of NaI for $LaCl_3$(Ce), to ~1.5 times that of NaI for $LaBr_3$(Ce). The intrinsic radiation for the lanthanum halides for the same crystal size is 200 times less than that of LSO, the energy resolution is at least two times better than NaI, and large crystals are already available commercially. These lanthanum halides are the likely near future in low-resolution scintillation spectroscopy.[10-15] Some results of testing and implementation of these scintillators for NDA measurements of special nuclear materials are presented here.

Improvements over NaI resolution are now available with room-temperature semiconductor detectors, although crystal size and commercial availability limit practical usefulness. The limits are a result of the characteristics of charge collection for these materials but are also influenced by the status of crystal-growth technology and understanding of the properties of these semiconductors. Advances in size and performance of non-cryogenic semiconductor CdTe and CdZnTe reflect improvements in the production of these materials, new technologies for surface contacts, the development of small electrical coolers, and advances in analog microcircuits.

Commercial, portable, electrically cooled CdTe detectors with crystals at least four times larger than those offered in the past are a new and truly portable alternative to Ge.[16] Implementation of portable CdTe for full, wide-range gamma-ray isotopics of plutonium, uranium up to 80% ^{235}U, and mixed (U-Pu) oxide[17-19] is now a commercial option. The thickness of CdTe is limited to a few millimeters by charge transport properties. Therefore, measurements must use the lower-energy portion of gamma-ray spectra. Both cost and delivery time are moderate for CdTe, compared to low for NaI, but the cooled CdTe detector is a high-resolution detector.

The introduction of the coplanar-grid electrode overcomes some deficiencies of charge collection in CdZnTe, enabling the development and optimization of such detectors in numerous adaptations of this approach with sizes much larger than CdTe.[20-22] Testing and implementation for NDA of special nuclear materials has continued, but despite promise the largest CdZnTe crystals available commercially remain high in cost and require very long wait periods. Multi-element CdZnTe and CdTe detectors compensate for the small sizes of compound semiconductor crystals – or for the scarcity and high costs of the largest crystals. This comes at the expense of the simplicity of designs with single crystals. Commercial prototypes have been developed.[23, 24]

Germanium detectors (Ge) still offer the state-of-the-art in energy resolution. Very large crystals are available commercially and have become more affordable with time. Because of energy resolution and availability in all sizes, most fixed gamma-ray NDA instruments use Ge when access to liquid nitrogen is not an issue. Commercial options for electrical cryogenic coolers for Ge detectors have become increasingly reliable, and are compact and packaged for portable use. Advances in signal processing increase both performance and effective lifetime of Ge detectors.[25-28] Portable Ge shielded by dense scintillator material is a dramatic step toward high-resolution spectroscopy for increased sensitivity and versatility in the most challenging environments.[29] Sensing transitions from superconducting states in supercooled materials is a distant-future option for very-high resolution that approaches the radiation line widths.

Imaging systems that utilize apertures with inorganic scintillators or employ crystal arrays, mechanically segmented crystals, segmented PMTs, *etc*. have been developed[30] and implemented in the field.[31-32] Others use Ge that is “position-sensitive”. Advances in technology for surface contacts and analog/digital circuitry add position sensitivity to Ge detectors through essentially continuous but electronically isolated multiple surface contacts that effectively segment the volume of a planar or coaxial Ge detector. Such detectors enable high-resolution imaging in the 4-π environment surrounding the detector via detection of multiple (three) Compton-scattering events.[33, 34] Imaging achieved in this way uses no aperture and interprets the source distribution in three dimensions. The readout of the Compton imager is a unique gamma-ray spectrum for each three-dimensional source voxel in the detector environment. Interpreting the position and energy of an individual Compton event within the Ge crystal requires analysis of relative pulse amplitudes for all surface-contact segments (10-to-100 contact segments for planar-to-coaxial crystals, respectively) as well as the

analysis of the pulse shapes in each segment. Interpretating the conical locus of the incident gamma trajectory from a sequence of three Compton events from the same gamma ray requires a logical reconstruction of the sequence of these Compton events. Interpretating the spectroscopic image for each gamma-ray energy requires analysis of the intersections of loci for the large number of events of a given gamma-ray energy required for such interpretation. Compton imaging has also been achieved at room temperature using a large CdZnTe detector with a pixelated anode for two-dimensional position sensitivity and analysis of pulse shapes for the third dimension.[35]

Advances in Ge materials now support development of prototype multiple-element Ge for the highest position resolution utilizing 4π Compton imaging.[36-38] These mechanically complex detectors consist of a stack of two-layer orthogonally-oriented narrow and thin Ge strips – up to ~100 strips per two-layer element with each strip read out at both ends. Variance on event position determined by strip pitch is small compared with that interpreted from the readout of a segmented Ge detector. However, operation at liquid-nitrogen temperature burdens the requirements for design, maintenance, and field applications of such mechanically and electronically complex detectors.

Currently, the use of arrays of small semiconductor detectors[39] is demonstrated in spectrometric DNS applications. The benefits of inorganic scintillators for DNS include the availability of crystals of almost any size and the existence of commercial support for needs such as stabilization. However, organic (plastic) scintillators may also emerge for DNS, preceding high-resolution gamma imagers, without or with apertures, in the maturity required for these applications. Plastic scintillators are lower in cost. The promise for these detectors is indicated by the demonstration of the enhanced photoelectric yield achieved by loading heavy elements into the plastic.[40] The spectrometer characteristics of these low-cost and rugged materials are presented in Section VIII. Promise for plastics in the designs of nanoparticulate detectors is on the more distant horizon.

Progress in gas-detector spectroscopy focuses on high-pressure xenon (HPXe) ion chambers.[41-46] This chapter illustrates benefits of HPXe such as insensitivity to changes in temperature,[47] and a factor-of-two improvement in resolution relative to NaI. This plus resistance to damaging effects of radiation encouraged the design and fabrication of several commercial prototypes. The benefits, along with convincing results from six years in the radiation fields of space,[48] are the promise for DNS in continuous NDA of nuclear materials if the manufacturing process succeeds in producing HPXe detectors that are sufficiently low in cost.

Table 1 summarizes the characteristics and performance of each of eight gamma-ray spectrometer detectors that are currently viable commercial options for NDA. Data for detectors that are available since the previous book[49] are included in bold along with data for those detectors that were described previously to emphasize advances in the recent fifteen years. The relevance of the information in Table 1 is discussed in the text below under the appropriate headings.

Much larger NaI(Tl) and Ge detectors are available than the corresponding entries in Table 1. Portable applications require shielded and collimated detectors that can be readily manipulated by hand throughout the plant. The weight of shielding is difficult to manage manually for detectors with areas that exceed ~5 cm^2. Including smaller-diameter NaI(Tl) and Ge detectors in Table 1 simplifies comparisons with newer detectors whose maximum dimensions are generally much smaller than the largest crystals of NaI(Tl) and Ge. The need to specify performance for at least two gamma-ray energies (122 and 662 keV) corresponds to common needs to measure ^{235}U, ^{239}Pu, and ^{238}U using gamma rays of 186-, 414- and 1001-keV, respectively.

Figures 1 and 2 are reference spectra of oxides of low- and high-burnup plutonium (93% ^{239}Pu and 64% ^{239}Pu, respectively). These spectra are measured using four of the detectors specified in Table 1: NaI(Tl) (NaI), co-planar-grid CdZnTe (CZT), electrically cooled CdTe (EC CdTe), and Ge.

The remainder of this report focuses on results obtained with the newer detectors with data appearing as bold entries in Table 1. Detailed discussions address the relevant detectors in each category. Results for certain less mature detectors with future potential, as well as others with potential that has been superseded by newer developments, are presented as well and compared with

the reference data in Table 1. The report also includes some discussion of the impacts of new supporting technologies that enhance the properties and performance of gamma-ray detectors.

II. SODIUM IODIDE AND OTHER ALKALI-HALIDE SCINTILLATORS

The most significant advances in *materials* for alkali halide scintillators are that NaI scintillator crystal spectrometers as large as 40 cm in length are now available from commercial manufacturers. Mechanisms for the production and collection of scintillation light using photomultiplier tubes (PMT) are discussed elsewhere.[50] Discussions in the remainder of this section on alkali halide scintillators as well as most of sections III and IV emphasize usefulness for NDA and, therefore, do not include all such scintillators.

The routine use of shielded compact NaI detectors for portable holdup measurements benefits from an ever-increasing variety (size, shape, spectral sensitivity, heat sensitivity…) of PMTs. This enables optimal mechanical matches with the smallest or largest scintillator and optimal spectral matches between the peak in the spectrum of scintillation photons (PHOTON PEAK λ in Table 1) and the peak in the spectrum of photocathode sensitivity. Newer, rugged, commercial NaI/PMT or CsI/PMT assemblies support acquisition of gamma-ray spectra with detectors that experience >200 G of mechanical shock during measurements performed during borehole drilling.

It is uncommon to implement scintillators in stand-alone NDA instruments because the higher resolution, the availability of liquid nitrogen in most NDA count-rooms, and a continuously decreasing cost differential between detectors with moderate-size Ge crystals and scintillation detectors make Ge an obvious choice. It is still not practical to implement Ge detectors in plant-wide portable applications. Therefore, many NDA needs for scintillators (NaI in particular) focus on portable applications. Fixed on-line installations of gamma-ray detectors in the plant (including DNS applications) are more likely to implement scintillators and other room-temperature detectors. Therefore, discussions of NaI in this section emphasize portable and on-line applications.

Fully optimized, NaI(Tl)/PMT detectors routinely give 6% resolution (FWHM at 662 keV). A similar light yield and emission-spectrum peak – 420 ηm compared to 415 for the NaI:Tl – plus a higher Z and 23% higher density of CsI(Na) compared to NaI(Tl)[51] make the CsI option a somewhat better choice for thin-crystal spectroscopic imaging. Nevertheless, newer lanthanum halides now offer even greater improvements over NaI, as described in section IV.

Table 1. Gamma-Ray Detector Properties and Performance[a]

DETECTOR	BGO ($Bi_4Ge_3O_{12}$)	NaI:Tl (compact)	$LaCl_3$:Ce (La:Ce::10:1)	$LaBr_3$:Ce (La:Ce::200:1)	Xe ($Xe:H_2$::200:1)	(CPG) CdZnTe (Cd:Zn:Te::1-x:x<0.1:1	CdTe (elect. cooled)	Ge (thick planar) (elect. or LN_2 cooled)
TYPE	scintillator	scintillator	**scintillator**	**scintillator**	**gas (ioniz. chamber)**	**solid-state**	**solid-state**	solid-state
DIMENSIONS: area (cm^2) × thick. (cm)	5 cm^2 × 2.5 cm (or larger)	5 cm^2 × 5 cm (or much larger)	**5 cm^2 × 5 cm (currently up to 20 cm^2 × 5 cm)**	**5 cm^2 × 4 cm (currently up to 20 cm^2 × 5 cm)**	**11 cm^2 × 7.5 cm (up to 100 cm^2 × 75 cm)**	**2.3 cm^2 × 1.5 cm (largest*)**	**1.2 cm^2 × 0.3 cm (largest*)**	5 cm^2 × 1.5 cm (or much larger)
VOLUME (cm^3)	13 (or larger)	26 (or much larger)	**26 (currently up to 100)**	**20 (currently up to 100)**	**83 (up to 7500)**	**3.5 (largest*)**	**0.4 (largest*)**	8
AVERAGE Z	28	32	**28**	**41**	**54**	**49**	**49**	32
DENSITY (g/cm^3)	7.1	3.7	**3.9** (van Loef 01)	**5.3** (van Loef 01)	**0.4-0.5** (Knoll 00 716)	**6.0**	**6.1**	5.3
RESOLUTION: % FWHM @ 662 keV [Intrinsic Photoel. Eff., %][b]	12% (Romano 99) [2.80]	7% (Vo 02a) [1.000]	**3.3%** (van Loef 01) *Commercial spec <4%* **[0.81]**	**2.8%** (van Loef 01) *Commercial spec <3%* **[0.40]**	**2%** (Bedding 03a) *Commercial spec <4%* **[0.20]**	**3.2%** (Vo 02a)** **[0.47]**	**0.6 %** (Vo 02a) **[0.10]**	0.2% Vo 02a [0.10]
RESOLUTION: % FWHM @ 122 keV [Intrinsic Photoel. Eff., %][b]	28% (Romano 99) [1.00]	13% (Vo 02a) [1.000]	***Better than NaI*** *Commercial spec ~8%.* **[1.00]**	***Better than NaI*** *Commercial spec ~7%* **[1.00]**	**7%** (Bedding 03a) **[0.95]**	**6.3%** (Vo 02a) **[1.00]**	**1.5 %** (Vo 02a) **[0.78]**	0.4% Vo 02a [0.81]
PHOTON PEAK λ (ηm)[c]	480	415	**330** (van Loef 01)	**360** (van Loef 01)	**NA**	**NA**	**NA**	NA
PHOTON DECAY τ (ηs)	300	230	**25 (60%) 210 (30%)**	**35 (90%)**	**NA**	**NA**	**NA**	NA
AVAILABILITY	~ 6 wks after order	~ 2 wks after order	**~ 4 wks after order**	**4-8 wks after order**	**?**	**~ 1 yr after order**	**~ 24 wks after order**	~ 4-8 wks after order

[a] Intrinsic properties of scintillator materials are from Knoll 00 235 unless noted otherwise.

[b] Calculated intrinsic photoelectric efficiency (normalized to NaI:Tl values: 1.000 at 122 keV and 0.150 at 662 keV) for stated thickness of detector whose resolution is quoted.

[c] Glass transmits down to 350 ηm. Quartz transmits down to 180 ηm. Commercial suppliers currently use glass-window PMTs.

* Larger detectors that use multiple crystal elements have been demonstrated. (Prettyman 00, Redus 04)

** Resolution at 662 keV improves to ~2.5% for thinner crystals.

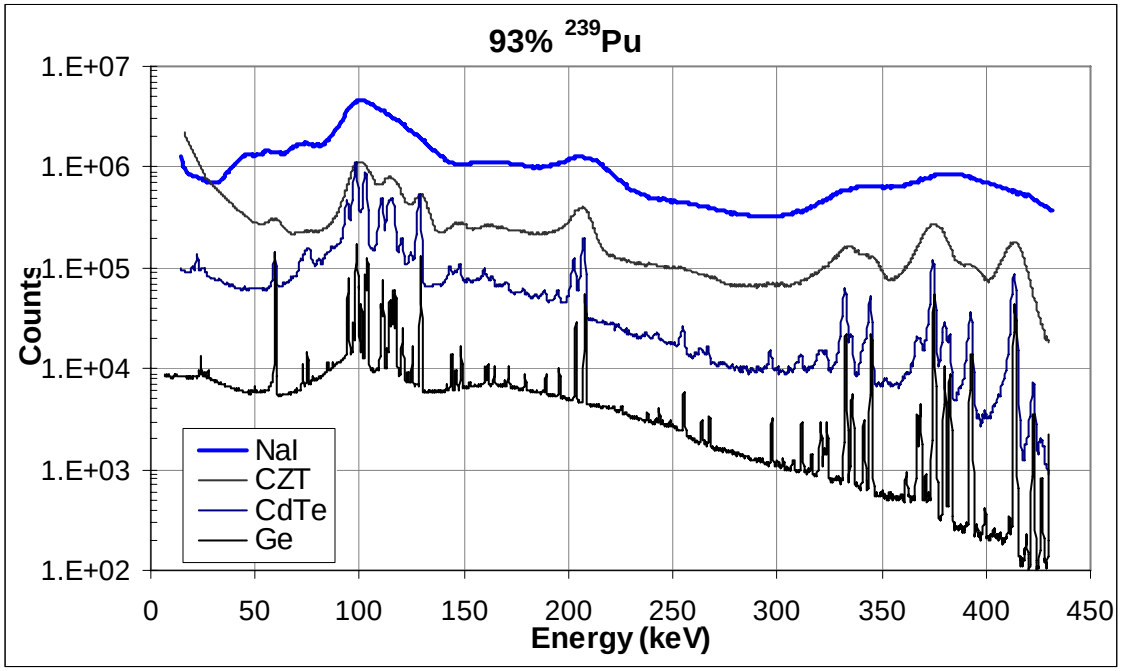

Fig. 1. Gamma-ray spectra of low-burnup (93% ^{239}Pu) plutonium measured with four different gamma-ray detectors: NaI:Tl, CPG CdZnTe, CdTe, and Ge (top to bottom). Refer to Table 1 for specifications on the detectors.

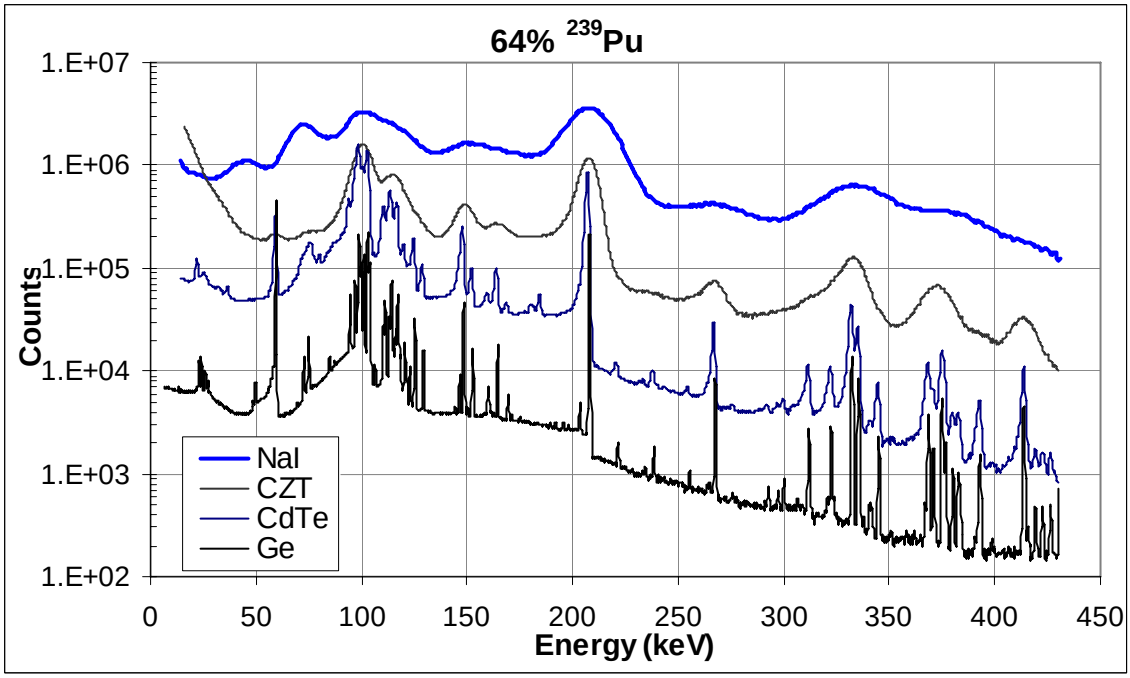

Fig. 2. Gamma-ray spectra of high-burnup (64% ^{239}Pu) plutonium measured with four different gamma-ray detectors: NaI:Tl, CPG CdZnTe, CdTe, and Ge (top to bottom). Refer to Table 1 for specifications on the detectors.

The peak wavelength of the NaI(Tl) scintillation light spectrum is 415 ηm (Tables 1 and 2) which is well-matched to the peak sensitivity of the most common bialkali photocathode material used in PMTs.[52] Table 2 indicates that the blue spectrum of scintillation light from CsI(Na) is much like that of NaI(Tl) with a nearly identical light yield. Table 2 also shows that the light yield of CsI(Tl) exceeds that of CsI(Na) by nearly 70%, but the scintillation light spectrum peaks in the green at 540 ηm. A modified photocathode with enhanced sensitivity at longer wavelengths may be used to optimize the performance of CsI(Tl).[53] Nevertheless, the scintillation spectrum of CsI(Tl) is also suited to use with silicon photodiodes, as discussed in section III.

Table 2. Alakalai Halide Scintillator Properties (Knoll 00 235)

DETECTOR	NaI:Tl	CsI:Na	CsI:Tl
TYPE	scintillator	scintillator	scintillator
Light Yield (photons/MeV)	38,000	39,000	65,000
AVERAGE Z	32	54	54
DENSITY (g/cm^3)	3.7	4.5	4.5
PHOTON PEAK λ (ηm)	415	420	540
PHOTON DECAY τ (ηs)	230	460 4000	680 (64%) 3340 (36%)

A major drawback of spectroscopy with any scintillator, including NaI, is the influence of temperature on the relative light output of (often multiple) scintillation decay modes. The result is a change in gain with temperature. Many commercial spectrometer systems stabilize against gain changes by empirically tracking gain drift and either compensating with analog adjustments of the gain or digital adjustments of the energy regions used to analyze the spectral data. Most scintillator stabilization is applied to NaI spectrometers. Newer intrinsic stabilization of scintillator gain against drift caused by temperature change[54] may widen the range of temperature suitable for use of these scintillators and extend applications to scintillators such as BGO with resolution significantly worse than that of NaI.

Alkali halide scintillators have been demonstrated for spectroscopic imaging with coded apertures.[55] The development of this technology has utilized both arrays of large (10-cm × 10-cm × 10-cm) NaI detectors and large-area (12-cm diameter by 1-cm thick) CsI(Na) scintillators coupled to position-sensitive PMTs.[56] A commercial version of the latter implementation of this imaging approach has been applied to measurements of in process plutonium inventory in a high-throughput, continuous system for aqueous dissolution of low-burnup plutonium.[57] Figure 3 shows the sketch of the dissolver and the two-dimensional spectroscopic image of ^{239}Pu superimposed on a photograph of the process equipment. Applications of this imaging system to in-process measurements of ^{235}U are also reported.[58] Both of these low-resolution applications would benefit from higher energy and position resolution available from a hybrid orthogonal-strip germanium detector[59] but with significant sacrifice in simplicity, as described in section V.

The NaI detector specified in Table 1 has a relatively small crystal, consistent with the other detectors listed. The quoted 7% energy resolution is nominal rather than optimum. Detectors of this size and performance are typical of those used in portable measurements of holdup and in-process nuclear materials.[60]

Figures 1 and 2 show the spectra of low- and high-burnup plutonium measured with this NaI detector and with three of the other detectors described in Table 1. The NaI energy resolution is the lowest of the four detectors. The 414-keV gamma-ray peak of ^{239}Pu appears as an unresolved shoulder on the high-energy side of a group of several peaks in these NaI spectra. The activity in the grouping of peaks is dominated by ^{239}Pu in the low-burnup spectrum but includes significant contributions from ^{241}Am and ^{241}Pu in the high-burnup spectrum. Either low-resolution response-function fitting[61] – which requires very long counts with good statistics – or a conservative setting of energy regions-of-interest[62] is required to use NaI in unbiased measurements of variable-burnup plutonium. Similar interference problems arise with NaI measurements of ^{235}U in most facilities.[63] A long count time is rarely an option in portable applications, and conservative settings give rise to systematic effects in quantitative results. These problems require portable detectors with better resolution than NaI. The important solutions to these problems include lanthanum halide scintillators and CdZnTe. These are discussed in sections IV and VI, respectively.

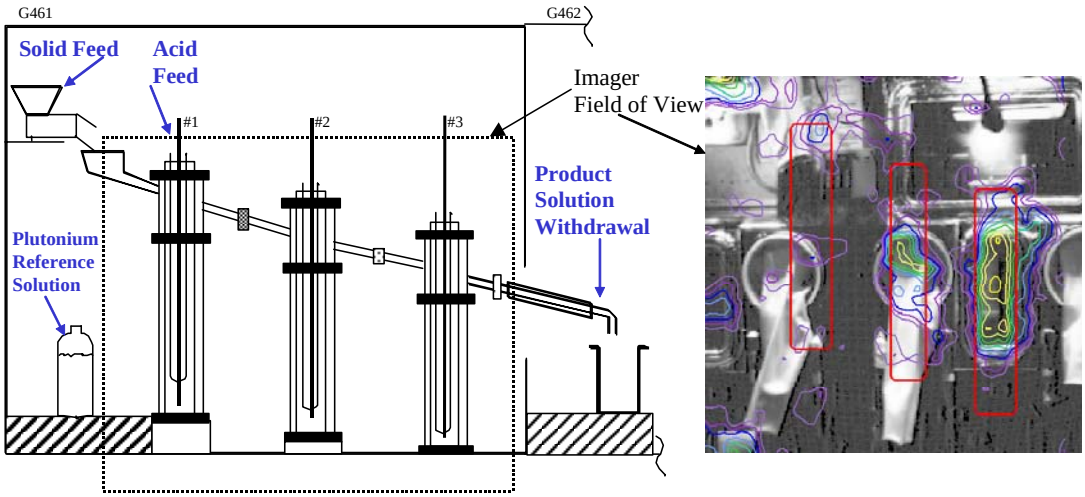

Fig. 3. Three aqueous dissolver columns in the field of view of the spectroscopic imager (sketch at left) are outlined in red in the photograph of the dissolver glove box (right). Colored contours (yellow-to-violet ≡ 900-to-100 counts) show the distribution of ^{239}Pu in the dissolver columns inside the glove box as measured in a 10-min count with the commercial imager. Contour data correspond to a 373-430 keV window in which ^{239}Pu activity dominates in the CsI(Na) spectrum.

III. SCINTILLATOR-PHOTODIODE DETECTORS

Semiconductor photodiodes are alternatives to PMTs for converting scintillation light to charge.[64] The discussion below focuses on efforts to improve the performance in the energy range of 100-1000 keV that is available with NaI(Tl)/PMT detectors with areas of ~5 cm^2.

Photodiodes are more rugged than PMTs, more compact, and unaffected by external electric fields. The thinnest wafer (<0.1 mm thick) of silicon is opaque to visible scintillation light and, under minimal bias, transports all primary electrons rapidly to the collection surface. The quantum efficiency (number of electrons per scintillation photon) of the silicon photodiode exceeds that of the bialkali photocathode by a factor of two to six, typically, for blue to green light (450-550 ηm). The higher yield of primary electrons results in a smaller statistical contribution to the energy resolution.

The high room-temperature thermionic emission caused by silicon's relatively small band gap (see Table 3) introduces a leakage noise that limits resolution, enforces the use of small-area devices, and adds temperature dependence to the resolution in addition to the scintillator's temperature-dependent gain. A lower-noise alternative to Si is a semiconductor material such as mercuric iodide, HgI_2, with a band gap that is twice that of Si. Results with these photodiode options are discussed below.

Table 3. Properties of Solid State Materials Governing Production of Charge

SOLID-STATE DETECTOR	(Average) Z	Density[a] (g / cm^3)	Band Gap[a] (keV)	Ioniz. Energy[a] (eV / e-h pair)
Ge	32	5.3	0.7[b]	2.98[b]
Si	14	2.3	1.1	3.6
CdTe	49	6.1	1.5	4.4
CdZnTe	49	6.0	1.6	4.3
HgI_2	62	6.4	2.1	5.0

[a] Values taken from Knoll 00 483

[b] Results for 77 K. (All others correspond to 300 K.)

Several commercial efforts to take advantage of the 70%-larger light yield of CsI(Tl) used 1-cm^2 Si photodiodes rather than a PMT to benefit from the higher quantum efficiency of the CsI(Tl). Although the resolution at 662 keV improves somewhat with CsI(Tl)/Si compared with NaI/PMT (~6% *vs*. the nominal 7% for NaI/PMTs), the CsI resolution at 122 keV is significantly worse than NaI because of leakage noise. Therefore, larger-area photodiodes required for use with larger (5-cm^2) CsI(Tl) scintillator crystals do not offer improved resolution compared with the NaI/PMT.

As a larger bandgap photodetector, HgI_2 has an advantage over Si of lower leakage noise at room temperature, although the larger ionization energy of HgI_2 reduces this benefit because of the corresponding statistical advantage of Si in primary excitation of electrons. The potential advantage is photodiodes of larger area than would be possible with Si. Commercial efforts implementing thin 1.6-cm^2 photodiodes of HgI_2 with CsI(Tl) scintillator crystals report ~5.6% FWHM at 662 keV.[65] Additional measurements that determined performance at 122 keV are documented in Table 4 for comparison with the performance of the nominal NaI detector. These data indicate a small resolution advantage at 662 keV over NaI/PMT for two CsI(Tl)/HgI_2 detectors. Nevertheless, the resolution at 122 keV is slightly worse than NaI. The reason is, in part, residual leakage noise despite the larger band gap; another contributor is the need for a longer amplifier shaping time for optimum resolution with CsI(Tl) because of its longer decay time. Optimum shaping time for CsI(Tl) is a compromise between the shortest possible to minimize noise and the longest practical to integrate the pulse.

An additional problem with HgI_2 is that even the thinnest photodiode is itself a gamma detector because of its large Z and density. Modeling may be required to determine the contribution of HgI_2 to a given measurement.

Table 4. Compare Prospective Portable Detectors with NaI

Detector		NaI:Tl/PMT *(Table 1)*	CsI/HgI_2 (smaller)	CsI/HgI_2 (larger)	CPG CdZnTe *(Table 1)*
122 keV	%FWHM	13	**15**	**15**	**6.3**
	%FWTM	25	**29**	**29**	**13**
662 keV	%FWHM	7	**5.8**	**6.0**	**3.2**
	%FWTM	13	**11.4**	**12.0**	**8.0**
% Rel. Intr. Photo. Eff.[a]	122 keV	100	**100**	**100**	**100**
$100 \times E / E$(NaI)	662 keV	100	**42**	**60**[aa]	**47**
Crystal shape		Cylindrical	**Rectangular**	**TRCC***	**Rectangular**
Crystal X-sectional area, cm^2		5	**1.6**	**8.6 to 1.3**[o]	**2.3**
Crystal depth, cm		5	**1.3**	**3.8**	**1.5**

[a] Calculated intrinsic photoelectric efficiency (normalized to NaI:Tl values: 1.000 at 122 keV and 0.150 at 662 keV) for stated thickness of detector whose resolution is quoted.

[aa] Used half of the stated thickness of the TRCC to obtain this result.

* Truncated Right Circular Cone (TRCC) with wide end facing the cylindrical collimator

[o] Range (maximum to minimum) of areas of TRCC

Although detector efficiency approaches that of the compact NaI/PMT detector, the data in Table 4 indicate that the CsI(Tl)/HgI_2 detector does not provide improvements over the performance of NaI/PMTs at either gamma-ray energy (122 and 662 keV). Coplanar-grid CdZnTe detectors and the lanthanum halides discussed in sections VI and IV do offer significant improvements.

Avalanche photodiodes amplify primary charge produced when scintillation light reaches the photodiode. These devices, which are documented elsewhere,[66] are also subject to limitations of leakage noise at room temperature. Advances in micro-cooler technology could revive photodiodes with resolution surpassing that available with PMTs.[67] Applications in NDA would include those requiring compact, low-noise, large-area and multi-crystal measurement systems.

Hybrid PMTs[68] utilize a primary photocathode of 5-cm^2-area or more combined with a very small (low-leakage-noise) secondary photodiode biased at a high voltage relative to the photocathode. Although the statistics of the primary production of charge are unchanged from that of the corresponding photocathode of a PMT, the statistics of the secondary production are greatly improved over that of the first dynode of a PMT.

Because the statistics of secondaries define resolution on multiple-photoelectron events, the hybrid PMT resolves single-, double-, and triple- (*etc*.) photoelectron events. This resolution supports diagnostics on statistics of charge production, as illustrated in Figure 4, which shows a few-photoelectron spectrum of the hybrid PMT measured at high gain plotted with a continuum spectrum measured at 50-times lower gain with a scintillator coupled to the hybrid PMT.[69] The data illustrate the advantage of the hybrid PMT as a spectroscopic tool for comparing primary *net* charge produced in the PMT coupled to different scintillators (variable materials, shapes/sizes, surface characteristics, *etc*.). End-use practicality for NDA is limited in that the relative cost of the hybrid PMT is high, and the equivalent in compactness is available with traditional PMTs. Benefits of few-photoelectron resolution rarely exist for end-use spectroscopy applications, which require good primary statistics.

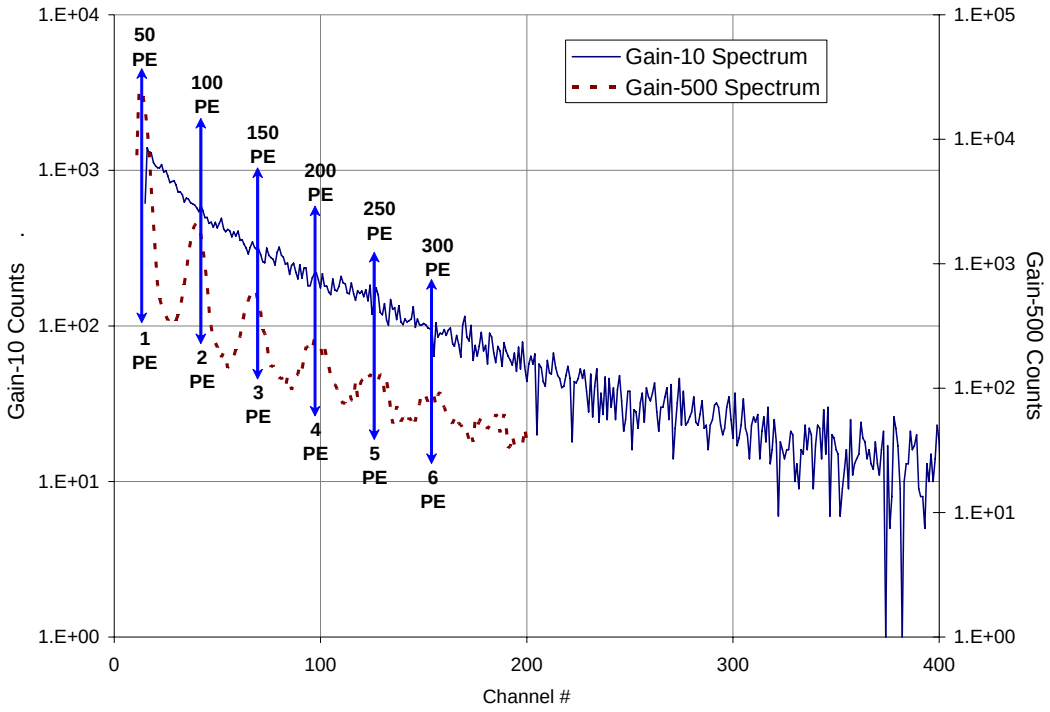

Fig. 4. The few-photoelectron spectrum of the hybrid PMT measured at high gain (dashed line) illustrates the resolution of successive multiple-photoelectron events. It also calibrates the number photoelectrons vs. channel in the spectrum measured at 50-times lower gain with a scintillator coupled to the hybrid PMT (solid line).

IV. INORGANIC LANTHANUM AND RARE-EARTH SCINTILLATORS

The appearance in the last decade of new "bright", relatively high-Z scintillators with densities that equal or exceed that of NaI is a most encouraging phenomenon regarding improvements over NaI/PMT detectors. This section focuses on results for the cerium-doped lanthanum halides compared with NaI/PMT detectors and for cerium-doped lutetium oxyorthosilicate[70, 71] (Lu_2SiO_5(Ce) or LSO) compared with BGO.

Some elemental components of the new materials have naturally occurring beta emitters. The following three are relevant to the discussions in this section:

- ^{176}Lu ($3 \cdot 10^{10}$ y, 2.6% of naturally occurring Lu).
- ^{142}Ce ($5 \cdot 10^{15}$ y, 11.1% of naturally occurring Ce).
- ^{138}La ($1.1 \cdot 10^{11}$ y, 0.1% of naturally occurring La).

Intrinsic background from ^{142}Ce is not significant, however. Relative to La, Ce is a 0.5-10% atomic species,[72, 73] and ^{142}Ce contributes minimally to intrinsic background from ^{138}La. Relative to Lu in LSO, Ce is a 0.055% atomic species,[74] and ^{142}Ce contributes minimally to background from ^{176}Lu. The contribution of intrinsic background from the decay of ^{176}Lu is not negligible.

A large crystal of LSO was tested along with BGO as a reference using a PMT with a bialkali photocathode. Table 5 compares this LSO scintillator with the reference BGO and NaI. (These data also appear in Table 1.) The density and light yield of LSO exceed that of BGO and the resolution is somewhat better. Considering that the spectrum of scintillation light is similar to that of BGO, even better performance than that observed for LSO is expected for a very good crystal of comparable size.[75] However, the need to subtract intrinsic background from LSO spectral data also contributes to the variance in the width of the net peak.

Beta decay of ^{176}Lu limits gamma-ray detection sensitivity in most of the useful energy range, and subtraction of the corresponding background affects the energy resolution. The gamma-ray spectrum of ^{137}Cs measured with BGO detectors and the intrinsic background spectrum for the LSO detector are shown in Figure 5. Also shown there is the net ^{137}Cs spectrum with background subtracted.

Because NDA for nuclear safeguards relies on gamma-ray measurements between 100 and 1000 keV, subtraction of the substantial intrinsic background (~12,000 s^{-1} for a crystal of the size of the LSO test crystal) will often determine the limiting sensitivity for measurements performed with LSO. The measured BGO spectrum includes no intrinsic background. Room background for the spectra plotted in Figure 5 is negligible. Given the substantial intrinsic background and relatively small advantages compared to BGO, LSO is not a compelling alternative to BGO.

Table 5. Compare LSO with BGO and NaI[a]

DETECTOR	**BGO** ($Bi_4Ge_3O_{12}$)	**NaI:Tl**	**LSO (Lu_2SiO_5:Ce)** (Lu:Ce::1800:1)
TYPE	scintillator	scintillator	**scintillator**
DIMENSIONS: area (cm^2) × thick. (cm)	5 cm^2 × 2.5 cm (or larger)	5 cm^2 × 5 cm (or much larger)	**32 cm^2 × 1.3 cm**
VOLUME (cm^3)	13 (or larger)	26 (or much larger)	**41**
AVERAGE Z	28	32	**25**
DENSITY (g/cm^3)	7.1	3.7	**7.4** (Ludziej 95)
Light Yield (photons/MeV)	8,200	38,000	**~20,000** (Ludziej 95)
RESOLUTION: % FWHM @ 662 keV [Intrinsic Photoel. Eff., %][b]	12% (Romano 99) [2.80]	7% (Vo 02a) [1.000]	**11%** (Romano 99) **[1.34]**
RESOLUTION: % FWHM @ 122 keV [Intrinsic Photoel. Eff., %][b]	28% (Romano 99) [1.00]	13% (Vo 02a) [1.000]	**23%** (Romano 99) **[1.00]**
PHOTON PEAK λ (ηm)	480	415	**420** (Knoll 00 244)
PHOTON DECAY τ (ηs)	300	230	**47** (Knoll 00 244)
AVAILABILITY	~ 6 wks after order	~ 2 wks after order	**n.a.**

[a] Intrinsic properties of scintillator materials are from Knoll 00 235 unless noted otherwise.

[b] Calculated intrinsic photoelectric efficiency (normalized to NaI:Tl values: 1.000 at 122 keV and 0.150 at 662 keV) for stated thickness of detector whose resolution is quoted.

Intrinsic background radiation of cerium-doped lanthanum halides is nearly two-orders-of-magnitude less than that of LSO for an equivalent scintillator mass. Coupled with resolution substantially better than that of NaI, material characteristics that equal or exceed those of NaI, and

rapid advances in the manufacture of these materials, lanthanum halides are very promising spectrometer alternatives.

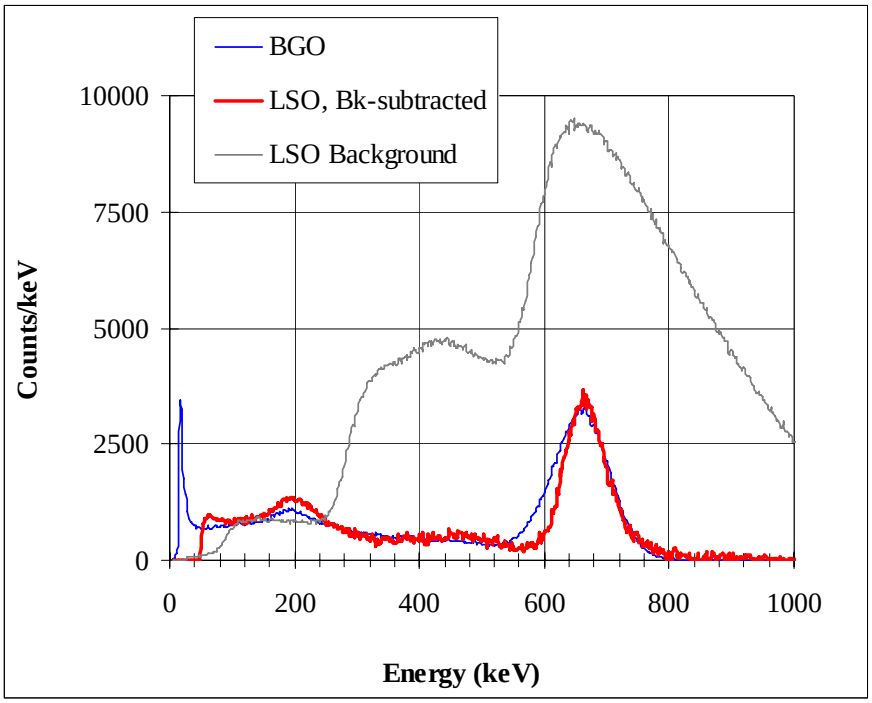

Fig. 5. The spectrum of ^{137}Cs measured with BGO detector and the intrinsic (^{176}Lu beta-decay) background spectrum for LSO are the thin blue and gray lines, respectively. The net gamma-ray energy spectrum of ^{137}Cs (measured spectrum minus intrinsic background) for the LSO detector is the heavy red line.

Table 1 indicates that the resolution of $LaCl_3(Ce)$ and that of $LaBr_3(Ce)$ at 662 keV are more than two-times better than that of NaI. The Z and density of $LaCl_3(Ce)$ are comparable to that of NaI. The Z and density of $LaBr_3(Ce)$ are 28% and 43% greater, respectively. Relatively large crystals (~100 cm^3) of both $LaCl_3(Ce)$ and $LaBr_3(Ce)$ are now available with short delivery times at moderate costs relative to NaI. The sizes of $LaCl_3(Ce)$ and $LaBr_3(Ce)$ crystals available commercially have increased steadily in the last two years. The performance of both $LaCl_3(Ce)$ and $LaBr_3(Ce)$ at 122 keV are nearly but not quite two-times better than that of NaI, as indicated in Table 2.

The factor-of-two or more resolution improvement of $LaCl_3(Ce)$ and $LaBr_3(Ce)$ at high energy is among the best results obtained with room-temperature gamma-ray detectors. The influence of surface nonuniformity has been noted, based on experimental data, as a possible cause of the smaller relative improvement in $LaCl_3(Ce)$ and $LaBr_3(Ce)$ resolution at lower gamma energy (122 keV) compared to NaI.[76]

Barium x rays following the decay of ^{138}La to ^{138}Ba by electron capture appear in long background spectra measured without a source. The x-ray peak observed at 37.6 keV (FWHM 6.4 keV) corresponds to the 37.4-keV K binding energy of barium. Barium x rays also follow the beta decay of ^{137}Cs to ^{137}Ba, and appear – with over an order-of-magnitude greater intensity than the background contribution – in each spectrum measured with a ^{137}Cs source. The x-ray peak at 32.8 keV (FWHM 8.3 keV) is an empirical average of barium K_α and K_β x rays, and its larger width reflects in part the energies of the barium K x rays. The energy difference of 4.8 keV between the internal and external x-ray peaks corresponds to an empirical average of the mostly undetected barium L_α and L_β x-ray energies. However, the contribution of the K x-ray energy distribution is not sufficient to explain the broadening of the external x-ray peak, relative to that of the x ray from intrinsic ^{138}La decay. The contribution of surface effects to worse resolution for x rays from the external source and for lower-

energy gammas in general is a solvable problem, and the low-energy x rays of barium are an indicator of surface quality for the lanthanum halide crystals.[77]

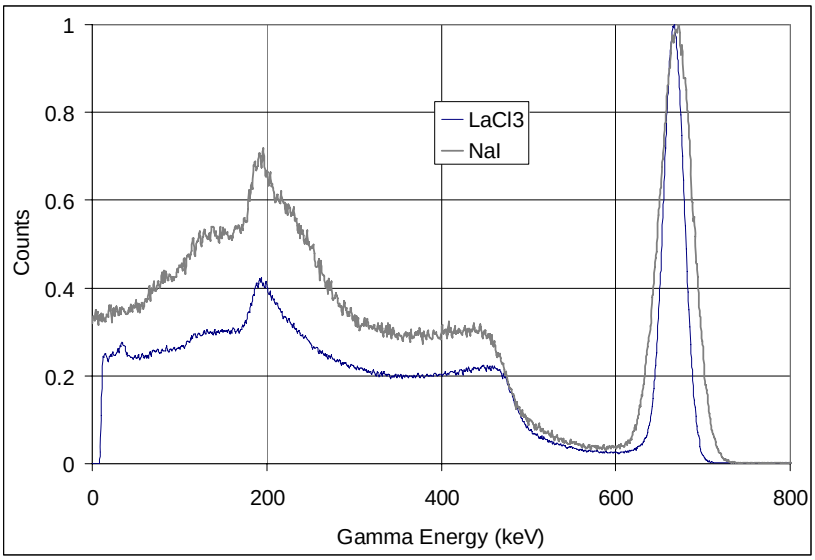

Fig. 6. Gamma-ray spectra of ^{137}Cs measured using a glass-window PMT with a 5-cm^2 by 2.54-cm thick $LaCl_3$(Ce) scintillator and the same-size NaI scintillator. The resolution (FWHM) at 662 keV is 3.9 and 6.9% respectively.

Figure 6 shows gamma-ray spectra of ^{137}Cs measured with a 5-cm^2 by 2.54-cm thick $LaCl_3$:Ce scintillator and with the same-size NaI.[78] Both spectra in Figure 6 were measured with a glass-window PMT. The relative FWHM at 662 keV is 3.9% for the $LaCl_3$ scintillator, not as good as the published results of 3.3% obtained with quartz-window PMTs (Table 1). This is partly a result of the loss of scintillation light from $LaCl_3$(Ce) below 350 ηm caused by absorption in the glass window of the PMT. The emission peak for $LaCl_3$(Ce) with 10% cerium doping is ~340 ηm. The higher wavelength emission peak (~380 ηm) of $LaBr_3$(Ce) with 0.5% cerium doping diminishes the effect of glass on the scintillation light incident on the PMT.

Figure 7 shows the gamma-ray spectra of 5-gram plutonium oxide samples of low-, medium- and high-burnup, measured with $LaCl_3$(Ce) and NaI detectors. Both use 5-cm^2 by 2.54-cm thick crystals and identical electronics.[79] Improved resolution with $LaCl_3$(Ce) at the 414-keV analysis energy for ^{239}Pu will contribute substantially to eliminating bias in measurements of high-americium materials.

Significant additional improvements (better energy resolution, and higher sensitivity because of higher density and Z, as indicated in Table 1) come with $LaBr_3$(Ce) crystals. The higher peak wavelength of the emitted photons compared with $LaCl_3$(Ce) (Table 1) gives $LaBr_3$(Ce) the additional advantage of better light transmission through the glass window of a PMT.

Relative to NaI, the cerium-doped lanthanum halides demonstrate improved performance and intrinsic properties for gamma spectroscopy applied to NDA of nuclear materials at high gamma-ray energies. Prospects for improved resolution at lower energies (below 200 keV) are good. The rapid advances achieved in materials production coupled with moderate costs and off-the-shelf availability of large crystals are strong indicators that cerium-doped lanthanum halides will replace alkali halides in the near future. Because of comparable performance, greater sensitivity, greater availability, and lower cost, the cerium-doped lanthanum halides should also compete favorably with CdZnTe and HPXe for NDA applications, including those described below for CdZnTe and HPXe that do not preclude the use of scintillators.

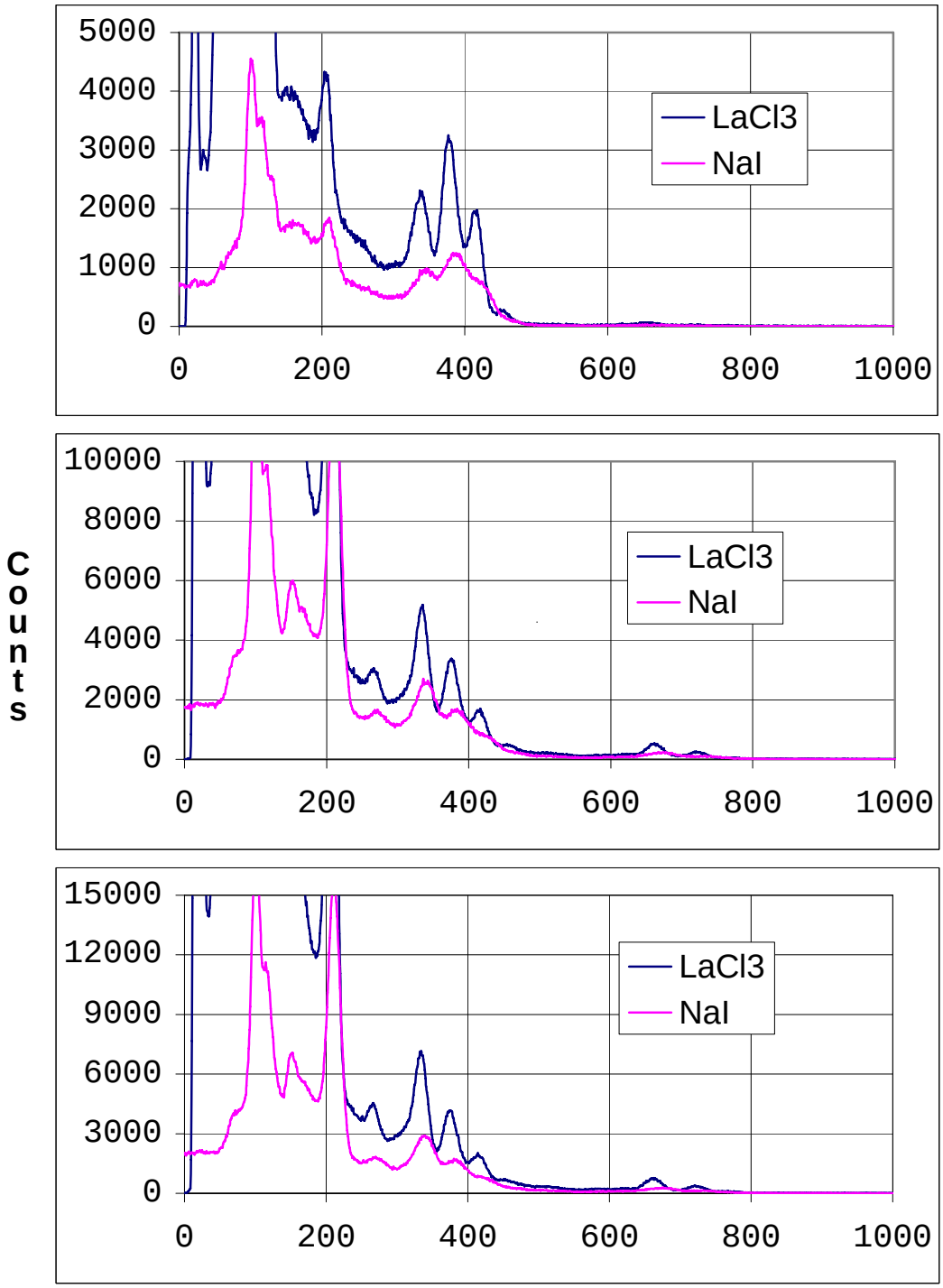

Fig. 7. The gamma-ray spectra, top to bottom, are those of low-, medium- and high-burnup plutonium (6%, 18% and 24% ^{240}Pu, respectively), measured with a 5-cm^2 by 2.54-cm thick ***LaCl$_3$(Ce)*** *scintillator and with the same-size NaI scintillator. The improved energy resolution at 414 keV is illustrated by the distinct peak in the LaCl$_3$ spectrum at this energy in the full range of isotopics.*

V. GE DETECTORS AND CRYOGENICS

Intrinsic germanium cooled to liquid nitrogen temperature continues to be the state-of-the-art in gamma-ray spectroscopy for NDA. Progress since the previous report on gamma-ray detectors for quantitative NDA[80] includes ready availability of very large Ge crystals, electrical cooling technologies, digital signal processing, advances in technology for surface electrical contacts, low-noise analog circuits, breakthroughs on semiconductor surface properties, and the implementation of active shields.

Table 1 includes specifications and performance data for a relatively small (5-cm^2 by 1.5-cm thick) planar Ge detector as a state-of-the-art reference for other spectrometer detectors of lower resolution described in the same table. Figures 1 and 2 show the spectra of low- and high-burnup plutonium measured with this Ge detector. The energy resolution for the Ge detector is the best of the four detectors represented in Figures 1 and 2, illustrating the complexity of these spectra.

A major advance for users who rely on high resolution with sensitivity in the widest energy range is that very large (up to ~300% efficient, relative to the efficiency of a 46-cm^2 by 7.5-cm-thick NaI detector, for detecting 662-keV gamma rays) Ge detectors are available and have become increasingly affordable. Applications to measurements of waste introduce additional criteria beyond those imposed by nuclear materials accountability, criticality safety, and radiation safety. These include requirements imposed by the Department of Transportation and by standards for acceptance of waste. Special nuclear materials represent only a fraction of the many isotopes that must be identified. Waste packages can be large with attenuating container walls. These applications benefit from high resolution and efficiency. Similar benefits accrue in NDA applications such as the security screening of freight.

More reliable, compact and vibration-free thermoelectric cooling extends field applications to measurements that cannot be supported by liquid nitrogen. Energy resolution for fixed electrically-cooled Ge is now comparable to that with liquid nitrogen cooling. The size of commercial electrical coolers has decreased, and the reliability and performance have improved significantly in the last ten years. Commercial portable electrically-cooled Ge detectors are also available now.

The gamma-ray spectra obtained with three high-resolution gamma-ray spectrometer systems are shown for low- and high-burnup plutonium oxide samples in Figures 8 and 9.[81] All three detectors can be used for gamma-ray isotopic measurements of low- to high-burnup plutonium and uranium. The liquid-nitrogen-cooled Ge detector gives the best energy resolution. Second-best is one example of a portable electrically-cooled Ge detector. The CdTe detector is discussed in Section VI.

Figure 10 shows a commercial, electrically-cooled, portable germanium detector. The weight (~10 kg without shielding and collimation) and dimensions are too large to be useful for measurements of deposits in plant equipment. These detectors can operate on a cart equipped with a lift mechanism to address many measurement needs from floor level. Nonetheless, needs for highly portable measurements of gamma-ray isotopics persist. The third set of data plotted in Figures 8 and 9 is that for a highly portable CdTe detector equipped with a small electric cooler. This detector has the resolution capability for the wide-range isotopics measurements.[82-83] However, because of the very small size of the CdTe crystal (the largest crystal size is indicated Table 1), implementation of CdTe isotopics excludes shielded materials. The first three detector columns of Table 6 give crystal dimensions and energy resolution for the three detectors used for Figures 8 and 9.

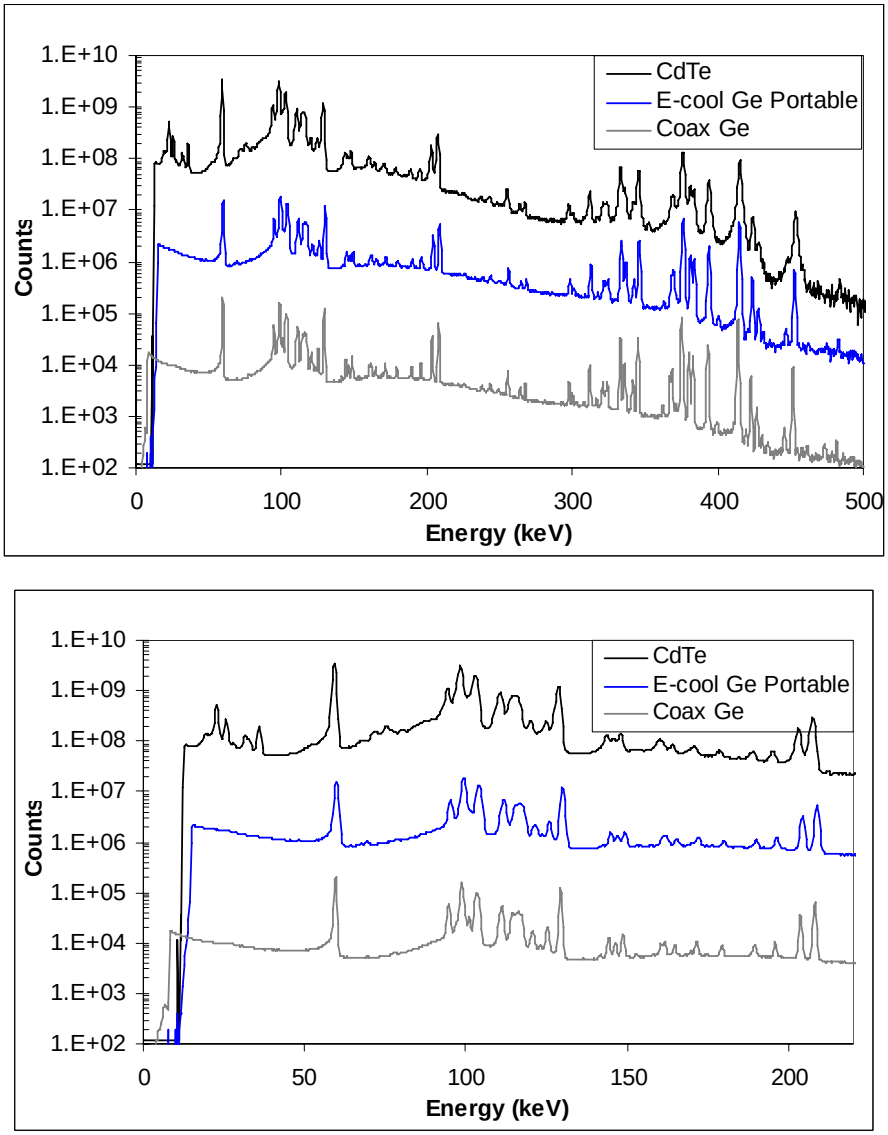

Fig. 8. High-resolution gamma-ray spectra of low-burnup (6% ^{240}Pu) plutonium oxide measured with a liquid-nitrogen-cooled coaxial Ge detector (bottom), portable electrically-cooled coaxial Ge detector (middle), and highly-portable cooled CdTe detector (top). Refer to Table 6 for crystal dimensions and energy resolution. The expanded view (0- 250 keV) shows the small resolution advantage of the portable electrically-cooled Ge over CdTe.

Figure 11 shows an innovative, prototype, portable Ge detector that uses a cylindrical Ge crystal surrounded by an active annular shield of dense BGO scintillator.[84] The packaging for this new electrically cooled detector is extremely compact, and its normal-use battery life exceeds 10 hours. Pulses from the Ge detector processed in anticoincidence with pulses from the 1-cm-thick BGO produce spectra with a suppressed Compton continuum increasing the sensitivity of measurements at low gamma-ray energies.

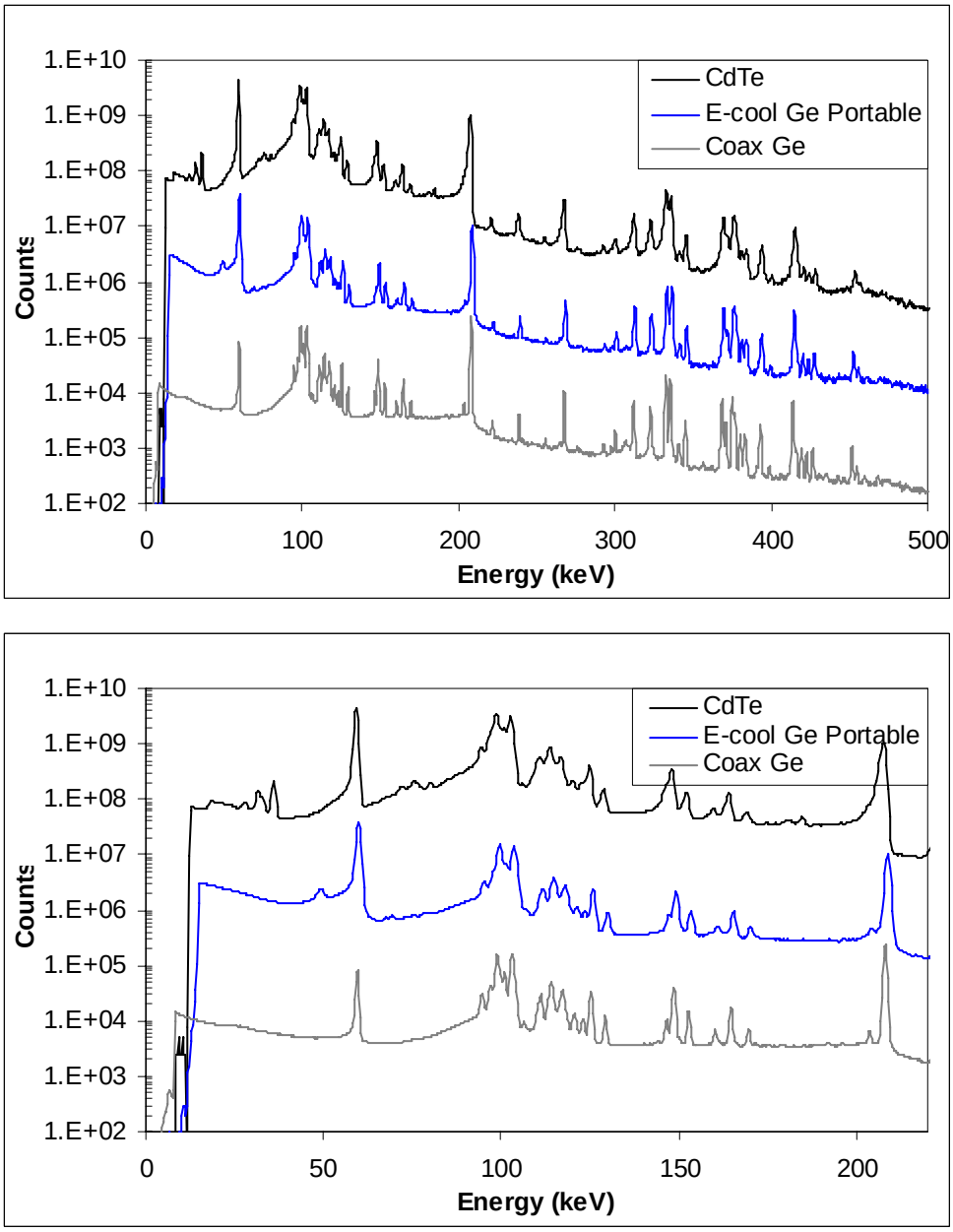

Fig. 9. High-resolution gamma-ray spectra of high-burnup (26% ^{240}Pu) plutonium oxide measured with a liquid-nitrogen-cooled coaxial Ge detector (bottom), portable electrically-cooled coaxial Ge detector (middle), and highly-portable cooled CdTe detector (top). Refer to Table 6 for crystal dimensions and energy resolution. The expanded view (0- 250 keV) shows the small resolution advantage of the portable electrically-cooled Ge over CdTe.

Applications of the prototype portable Ge detector with Compton suppression include measurements over a wide dynamic range. One example is low-enriched uranium, which often requires measurements of gamma rays at both 186- and 1001-keV. Another is uranium in reactor-return (recycled) material with high-energy gamma-ray activity (the 2614-keV gamma ray of ^{208}Tl) from decay of the ^{232}U progeny. The 1-cm-thick BGO annulus is also an effective passive shield, absorbing 100% of gamma rays at 122 keV and 50% at 662-keV.

Table 6. Compare High-Resolution Gamma-Ray Detectors

Detector		Ge, thick planar *(See Table 1)* LN_2 cooled	~14% Ge Portable Elect. cooled	CdTe *(See Table 1)* Highly portable elect-cool	$Ge/BGO_{anti\text{-}Compton}$ Very Portable, Elect. cooled
% FWHM	122 keV	0.4%	**1.3%**	**1.5%**	**TBD**
	662 keV	0.2%	**0.6%**	**0.6%**	**TBD**
% Intrinsic Photo. Eff.[a]	122 keV	81%	**~96%**	**63%**	**100%**
	662 keV	1.4%	**~3%**	**1.0%**	**5%**
Crystal shape		Planar	**Coaxial**	**Rectangular**	**Coaxial**
Crystal X-sectional area, cm^2		5	**~20**	**1.2**	**5.0**
Crystal depth, cm		1.5	**~3**	**0.3**	**5.0**

[a] Calculated intrinsic photoelectric efficiency at the given gamma-ray energy for stated detector thickness

The last detector column of Table 6 compares design parameters of this prototype portable Ge detector with the three commercial high-resolution detectors. The weight of the unshielded commercial portable Ge detector in Figure 10 exceeds that of the new prototype by nearly 40%. Target applications include highly portable, low-background, wide-energy-range, gamma-ray isotopics for low- to high-burnup plutonium and low- to high-enriched uranium. Achieving energy resolution sufficient for gamma-ray isotopics is the design challenge.

Fig. 10. The portable electrically-cooled Ge detector with tungsten collimator is shown mounted on a docking station (rectangular base) used for charging and cool down. The weight without the docking station is 12 kg.

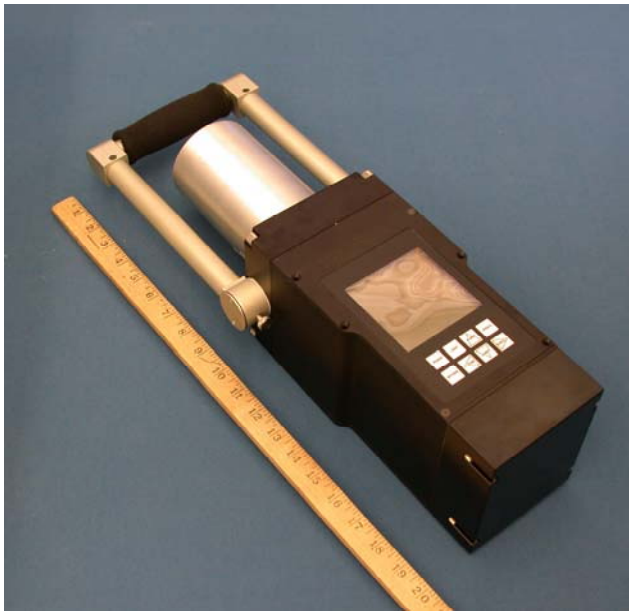

Fig. 11. The GN-5 prototype instrument (Frankle 03) is a self-contained compact high-resolution gamma-ray spectroscopy system. It incorporates an electrically-cooled Ge detector and a BGO anti-Compton annulus for high sensitivity in portable applications.

Micro-calorimetry defines a new field of super-high-resolution gamma-ray spectroscopy. Cryogenic cooling at liquid-nitrogen temperatures, ~77 ^{o}K, permits measuring the energy deposited by individual gamma-ray interactions into multiple discrete electronic transitions of a medium. Statistics of the primary electronic excitation limits energy resolution. When detector materials are cooled by mechanical and magnetic refrigerators to superconducting temperatures, ~0.1 ^{o}K, an individual gamma-ray interaction excites many more transitions (of much lower energy) from states of superconductivity to states of normal conductivity. Measuring the corresponding change in properties related to material conductivity determines the energy deposited by the gamma ray, but energy resolution is now limited by the thermal noise effects, which are very small at the low temperature and by intrinsic line widths.[85-86] Such energy resolution would enable gamma spectroscopy that is effectively independent of the limitations of continuum background and spectral interference. Research underway in micro-calorimeters for gamma-ray spectroscopy gives energy resolution of 42 eV at 103 keV, ten times better than germanium (see Figure 12).[87-88]

Digital signal processing (DSP) is responsible for major improvements in the resolution and throughput of germanium detector systems. The DSP spectrometer digitizes the preamplifier pulse directly, eliminating the linear amplifier. The advantages of this technology, combined with ever-increasing microprocessor memory and speed, include the ability to optimally process a wide dynamic range of pulses. Substantial benefits are realized in the performance of large Ge detectors that are sensitive to high gamma-ray energies and count rates. The spectral quality achieved with commercial DSP multichannel analyzers (MCAs), both benchtop[89] and portable,[90] consistently exceeds that of analog counterparts.

Substantial benefits of DSP are also realized in the performance of noncryogenic solid-state detectors such as CdZnTe and CdTe that are often implemented as portable spectrometers. The performance of these detectors is dependent on the choice of time constants for detector pulse processing. Portable DSP MCAs offer a wide range of time constants, while portable analog MCAs typically offer only a few choices.

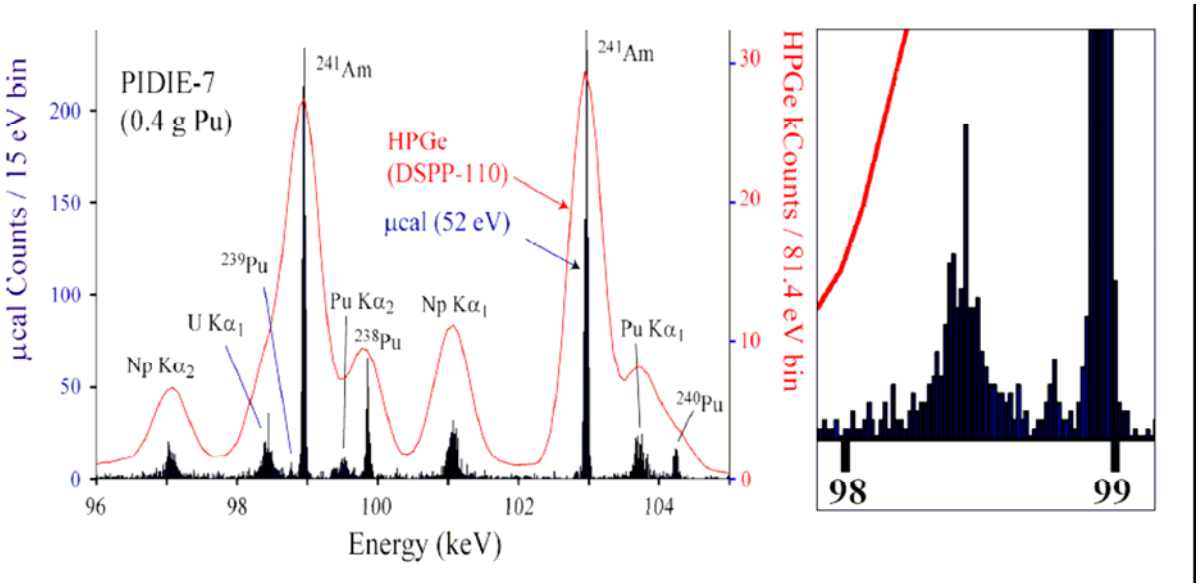

Fig. 12. LANL-NIST X-ray and gamma ray spectrum of Pu in the 100 keV region. Red spectrum taken with HPGe detector with ~500 eV FWHM resolution.. Black spectrum taken with single-pixel microcalorimeter detector with 52 eV FWHM resolution. In the microcalorimeter spectrum, we can identify by eye the U, Pu, and Np X-rays and the isotope-specific gamma rays from 238Pu, 239Pu, 240Pu, and 241Am. On the right, a magnified view of the 98 to 99 keV region, showing the 239Pu in between the U K-alpha X-ray and a very intense 241Am gamma ray. Note that the natural line shape of the Xrays is apparent in the microcalorimeter spectrum.

The impact of DSP on energy resolution is substantial, improving it by up to 50% for large coaxial detectors and high gamma-ray energies when compared analog signal processing with the same energy and detector. The reason is that the analysis of the digitized pulse can compensate to a greater extent for large ballistic deficits in large crystals.[91] Furthermore, data throughput can improve by 300% at high rates that demand shorter analog shaping times.[92] An additional benefit of DSP is that the lifetimes of Ge detectors operating in constant neutron environments can be extended because the analysis of the digitized pulse is less sensitive to changes in pulse shape caused by neutron damage.

Section I gave an overview of germanium detectors used for uncollimated high-resolution 4-π spectroscopic imaging of nuclear materials. Applications of low-energy-resolution aperture imaging to quantitative NDA were discussed in Section III. The benefits of improved energy and position resolution are greater sensitivity and accuracy, but such benefits may not outweigh the cost and maintenance of a cryogenic, hybrid, orthogonal-strip, germanium detector.[93] The implementation of high-resolution, uncollimated, 4-π Compton imaging may be worth the additional investment because of the potential for determining the three-dimensional distribution of isotopics. Most field applications of portable gamma-ray measurements are performed at hundreds or thousands of locations with low resolution, and many are performed in areas with a wide range of isotopic composition. Low-cost spectrometers (Section VIII) may replace many portable measurement needs in DNS implementations. A fixed installation of high-resolution spectroscopic imaging in these areas could greatly reduce the uncertainty caused by assumed stream values for the isotopic distribution at each particular measurement location in both portable and DNS implementations.

Cryogenic cooling is the major contributor to the cost and maintenance of high-resolution gamma-ray spectroscopic imaging. Demands on electronics, algorithms for processing digital pulses, algorithms for interpreting pulse data, logic that defines event sequence, and algorithms for Compton imaging add requirements to the overall investment. Position-sensitive Ge detectors, electronics, and firmware are currently commercial prototypes.

"Segmented" germanium detectors use a single crystal with electronically isolated surface contacts that segment the volume of a detector.[94, 95] Interpreting the position and energy of each of three Compton-scattered events gives a three dimensional spectral image of the gamma-ray sources. Such detectors used in uncollimated applications of gamma-ray Compton spectroscopic imaging rely on new technologies for electrical contacts, low-noise analog preamplifiers, and fast, multichannel, digital pulse processing. Because noise determines the minimum variance in energy and position, cooling of the individual field-effect transistors is a feature that adds complexity to the detector design and increases failure possibilities. Segmentation of this type has also been achieved at room temperature with a cadmium zinc telluride detector to give position in two dimensions using multiple contacts (pixelated anode) on one surface of the rectangular crystal. Compton imaging in three dimensions is achieved by timing of gamma-ray pulses to determine the third coordinate of the interaction position within the crystal.[96]

Orthogonal germanium strip detectors have equivalent complexity of cryogenic cooling but offer improved position resolution in Compton imaging. Although the interpretation of position is simplified in these detectors relative to segmented germanium, they rely on additional material advances such as "amorphous" Ge to eliminate dead layers on the surfaces of narrow germanium strips.[97-99] Sacrificing the higher density of germanium in favor of orthogonal Si strip detectors has several major advantages for Compton imaging. Eliminating cryogenic cooling is among these, as is the maturity of orthogonal silicon strip detectors and the supporting electronics. Although orthogonal silicon strip detectors are most likely for early NDA implementation of high-resolution Compton imaging, another decade may pass before such systems are available for testing.

VI. NONCRYOGENIC PORTABLE SEMI-CONDUCTOR DETECTORS

When large crystals are not required, compound semiconductor materials are potential alternatives to Ge if compromises in resolution are acceptable, and to NaI when better resolution is required. Progress in solid-state gamma-ray detectors that use such materials is significant, and it is far from complete. This section indicates some of the parameters that influence resolution and limit crystal size in compound semiconductors. More detail is published elsewhere.[100]

The production of highly pure elemental semiconductors (Ge and Si) benefits from decades of effort. Development of compound semiconductors is less mature. Compound materials are subject to effects of additional impurities. Furthermore, charge-transport properties of pure compound semiconductors are less ideal than those of Ge or Si, and impurities increase problems from charge trapping. Finally, order-of-magnitude differences between drift velocities of electrons and holes in compounds contrast with very similar drift velocities in Ge and Si.[101] These effects limit the practical crystal size by crystal-growth and charge-transport limitations. Resolution is impacted by all charge-transport issues.

Several material parameters influence energy resolution in solid-state detectors. One is the band gap. Resolution improves as the band gap decreases because more charge is created for a given amount of energy deposited. Table 3 indicates that Ge should give the best resolution based on its smaller band gap. However, resolution also improves with reduction of noise from charge leakage as the band gap decreases. Therefore, high Ge resolution is only possible with cooling to liquid nitrogen temperatures to eliminate thermal noise effects. A qualitative look at the three compound semiconductor materials in Table 3 suggests that CdTe, with the smallest band gap is capable of the best energy resolution of the three and that HgI_2 with the largest band gap, is best-suited for room-temperature operation, both of which are validated empirically. The resolution of these compound semiconductor materials is intermediate between NaI and Ge.

Table 7 describes performance, as well as efficiency and size of the largest available crystals of three noncryogenic, commercial, semiconductor detectors: coplanar-grid cadmium zinc telluride (CPG CdZnTe), electrically cooled cadmium telluride (CdTe), and mercuric iodide (HgI_2). Figure 13

is a plot of the intrinsic photoelectric efficiency as a function of energy. This section discusses these three detector types. Also included as reference data in Table 7 is the corresponding information for a portable electrically cooled Ge detector and a compact NaI.

Table 7. Compare Non-Cryogenic Portable Solid-State Gamma-Ray Detectors

Detector		~14% Ge *(See Table 6)* Portable elect-cool	(CPG) CdZnTe *(See Table 1)*	CdTe *(See Tables 1 & 6)* Highly portable elect-cool	HgI_2[b]	NaI:Tl *(See Table 1)*
% FWHM	122 keV	1.3%	6.3%	1.5%	~5%	13.0%
	662 keV	0.6%	3.2%	0.6%	3-4%	7.0%
% Intrinsic Photo. Eff.[a]	122 keV	~96%	100%	63%	97%	100%
	662 keV	~3%	8%	1.0%	5%	15%
Crystal shape		Coaxial	Rectangular	Rectangular	Rectangular	Cylindrical
Crystal X-sectional area, cm^2		~20	2.3	1.2	6.3	5.0
Crystal depth, cm		~3	1.5	0.3	0.3	5.0

[a] Calculated intrinsic photoelectric efficiency at the given gamma-ray energy for stated detector thickness

[b] http://www.contech.com/Mercuric_Iodide_Detectors.htm

CPG CdZnTe

The development and production of cadmium zinc telluride material[102] and the design and manufacture of detectors that use these crystals[103-107] have taken place since 1985. Stoichiometrically, the material is typically $Cd_{1-x}Zn_xTe_1$, where $0<x<1$.[108] The difference of pulses from coplanar,

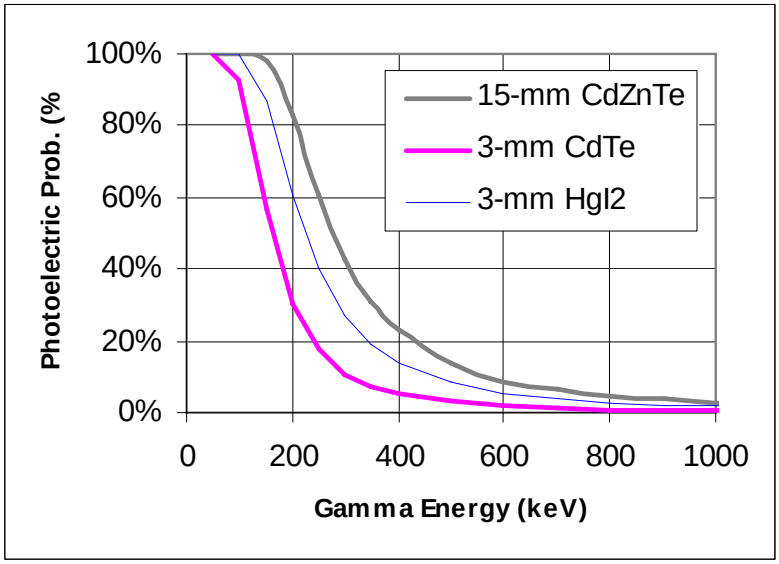

Fig. 13. Intrinsic photoelectric detection efficiency vs. gamma-ray energy for the three compound semiconductor detectors listed in Table 7: the 15-mm-thick CPG CdZnTe (top, gray), 3-mm-thick CdTe (middle, blue), and 3-mm-thick HgI_2 (bottom, pink) detectors.

differentially biased anodes (coplanar-grid or CPG) compensates for the nearly order-of-magnitude difference in transport mobility of electronics and holes in solid-state material.[109, 110] Timing between anode and cathode pulses determines interaction depth, which permits correction for the loss of charge from recombination or trapping effects.[111, 112] A large band gap compared to Ge and Si permits operation of CdZnTe at room temperature. Commercial CdZnTe and CPG CdZnTe detectors are used in portable and DNS applications.[113-117]

The largest CPG CdZnTe detectors are limited in size (cubic crystals 1.5 cm on a side) and have a lower intrinsic efficiency at 662 keV than the compact NaI detector in table 7. However, this detector

is approximately equal in sensitivity to the 2.5-cm-diameter compact NaI detector in many portable measurement applications because the ratio of peak-to-Compton ratio for the CdZnTe exceeds that of NaI. Resolution advantages of CPG CdZnTe over NaI, illustrated in Figures 1 and 2 and Table 7 are also essential in many common interference situations. A CPG CdZnTe detector usually:

- resolves the ^{239}Pu 375-keV complex (which is often dominated by activity from ^{241}Am) from the 414-keV peak of ^{239}Pu.
- permits measurements of ^{235}U at 186 keV in the presence of plutonium.
- resolves the ^{235}U 186-keV peak from the 238-keV peak – from the decay-chain of ^{232}U – that appears in spectra of recycled material.
- resolves 414-keV and other gamma rays (including 345 keV) of ^{239}Pu from lower-energy ^{237}Np gamma rays (especially at 300 keV) to permit evaluation and extraction of less intense but interfering ^{237}Np activity at 416 keV.

The large CPG CdZnTe detector is pictured alongside the compact NaI detector in Figure 14 to illustrate the similar dimensions. The benefits of its superior energy resolution are, unfortunately, outweighed by the high cost of the large CPG CdZnTe detector and by its limited availability.

Electrically Cooled CdTe

Cadmium telluride material properties have improved since 1985. Charge transport problems limit the detector thickness to 3 mm. Although the relatively large band gap (Table 3) permits operation at room temperature, a great advantage in energy resolution is achieved by cooling to just below zero degrees Centigrade because the thin crystals are most useful for spectroscopy at lower gamma-ray energies (< 200 keV) where the noise reduction is very beneficial. Simple circuitry that analyzes pulse shape can be used to assess corrections for charge loss. Both cooling and charge-loss corrections are implemented in commercial CdTe detectors.

Figure 13 and Table 7 show the significant difference in the intrinsic detection efficiency of the largest CdTe and CPG CdZnTe detectors. Because of its small size, the CdTe detector is not practical for measurement of holdup deposits that must use higher-energy gamma rays and many very short counts. However, its good energy resolution –comparable to Ge and five times better than that of CPG CdZnTe – contributes greatly to portable measurements of isotopics.

Fig. 14. The CPG CdZnTe, compact NaI, and CdTe detectors (Table 7) pictured at the left, center, and right, respectively. The rectangular module at the right is the power supply for the Peltier cooler within CdTe detector.

The recent commercial availability of Peltier-cooled CdTe detectors with crystals larger than 1 cm^2 has made gamma-ray isotopic measurement of uranium and plutonium truly portable.[118-120] Figures 1, 2, 8, and 9 illustrate the high resolution of these detectors which operate with automated charge-loss corrections. The energy resolution of the best cryogenically cooled Ge detector is only three times better than that of CdTe. Figures 14 and 15 illustrate the compact dimensions of the CdTe detector and its portable power supply.

The capability of CdTe to analyze the isotopic distribution over a wide range (3%-30% ^{240}Pu and higher), (0.1 to 80% ^{235}U), and mixed oxide. A count time of 15 min. with the CdTe detector measures ^{240}Pu to 2% and ^{235}U to 3%. Figure 15 shows the CdTe detector in use for gamma-ray isotopics measurements of plutonium.

The current large-area, single-crystal CdTe detector is too thin (< 0.3 cm) for practical measurements of holdup. A CdTe thickness of 0.2 cm absorbs 36% of ^{235}U gamma rays at 186 keV but only 12% of ^{239}Pu gamma rays at 414 keV. However, new commercial efforts to develop prototypes composed of stacked CdTe[121] crystals may triple the effective CdTe thickness. Higher noise from the multielement detector will preclude use of the crystal array for gamma isotopics measurements, but the possibility exists for analyzing pulses from the first layer for isotopics while using the full stack to quantify holdup using higher-energy gamma rays.

Fig. 15. A Peltier-cooled CdTe detector and DSP MCA in use for isotopics measurements Pu in a glove box.

Measurements of ^{235}U at 186 keV as well as those of ^{239}Pu, ^{241}Pu, and ^{238}Pu at 129, 149 and 153 keV, respectively, have the advantages that they are intense and easily shielded from room background. Low- or intermediate-resolution measurements of ^{239}Pu using the 414-keV gamma ray require meticulous attention to the determination of room background at each location because no practical shield is thick enough to effectively eliminate gamma rays of this energy. This is not the case for the lower-energy gamma-ray region. Hence, portable gamma-ray measurements of plutonium using the current large-area, single-crystal CdTe detector would be simplified compared to measurements with low- or intermediate-resolution detectors that are unable to resolve gamma rays or sensitively extract peaks from the larger continuum in the lower energy region. Such applications require nuclear materials that are not heavily shielded.

HgI_2

Because of its relatively large band gap (see Table 3), mercuric iodide, HgI_2, is viable at room-temperature as a semiconductor detector. Like other compound semiconductors, charge-transport properties of this material limit the thickness of useful crystals. Mercuric iodide crystals with areas up to 6.3 cm^2 and thickness up to 3 mm are now available with performance indicated in Table 7. A larger area compared to that of the largest CPG CdZnTe detector (2.3 cm^2) is possible without sacrificing energy resolution in part because of the band-gap advantage of HgI_2 discussed in Section III. However, the coplanar grid also contributes additional noise to the CdZnTe pulses. Even 0.1-mm-thick crystals of HgI_2 have reasonable intrinsic absolute photoelectric efficiency at 100 keV (Figure 16) because of their relatively high density and Z (Table 3). The efficiency of the 3-mm-thick HgI_2 detector is better than that of the thickest CdTe detector and approaches that of the thickest CPG CdZnTe detector (Figure 13). Published results (Vaccaro 01) indicate that improved materials give long-term spectral stability not demonstrated previously for HgI_2. Nonetheless, HgI_2 detectors are not included in Table 1, because i) both energy resolution and detection efficiency for large HgI_2 detectors are only comparable to that of the CPG CdZnTe detector (Table 7), ii) the cost of large HgI_2

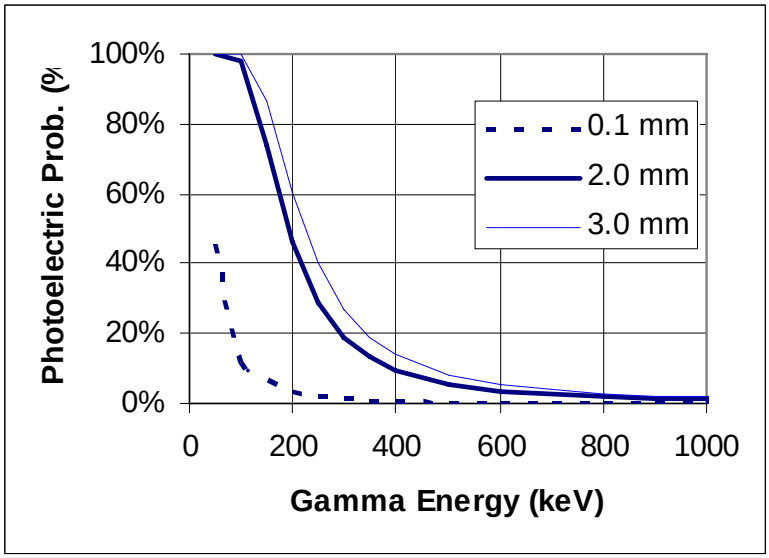

Fig. 16. The intrinsic photoelectric detection efficiency is plotted vs. gamma-ray energy for three thicknesses of mercuric iodide. The thinnest (dashed line) is comparable to a photodiode (Section III).

detectors exceeds that of large CPG CdZnTe detectors, which is already high, iii) there is little field experience with large HgI_2 detectors, and iv) the availability of large HgI_2 detectors is unknown.

VII. GAS-FILLED DETECTORS: HIGH-PRESSURE XE IONIZATION CHAMBERS

The benefits of gas detectors include long-term stability that cannot be equaled by scintillator or solid-state detectors because charge transport properties of gas are not significantly impacted by changes in temperature and the effects of radiation. Stability is a highly desirable characteristic for detectors in unattended monitoring applications, perhaps where climate and radiation vary. High-pressure xenon ionization chambers have emerged recently as gamma-ray spectrometers.[122]

High-pressure xenon ion chambers (HPXe) are cylindrical tubes with a concentric-wire or -rod anode. Most are equipped with a cylindrical Frisch grid[123] that surrounds the anode. The large difference in drift velocity of electrons and positive xenon ions causes the measured pulse amplitude to be sensitive to the interaction position in an ungridded ion chamber. However, the electrostatic

effect caused by vibration and the resulting change in the relative positions of the differentially biased anode and grid is a source of noise. Despite high bias voltages, charge collection time is long in xenon gas, and a long amplifier shaping time is required.

Commercially available HPXe detectors are intermediate-resolution gamma-ray spectrometers. Xenon's high atomic number (Z=54) and resulting high photoelectric cross-section are useful for high gamma-ray energies. Its density is approximately 0.4 g/cm^3. The detectors are available with diameters of 3-11 cm. Figure 17 plots the intrinsic photoelectric efficiency for a 5-cm-thick compact NaI detector, a 1.5-cm-thick (largest) CPG CdZnTe detector, and a 10-cm-diameter HPXe detector with a gas pressure of 0.4 g/cm^3. The similar intrinsic efficiency of the HPXe and CdZnTe detectors is overcome by the larger size of the HPXe, whose overall length can be 10-100 cm compared to 1.5 cm for CdZnTe. Figure 18 shows a small-diameter, commercial prototype HPXe detector.

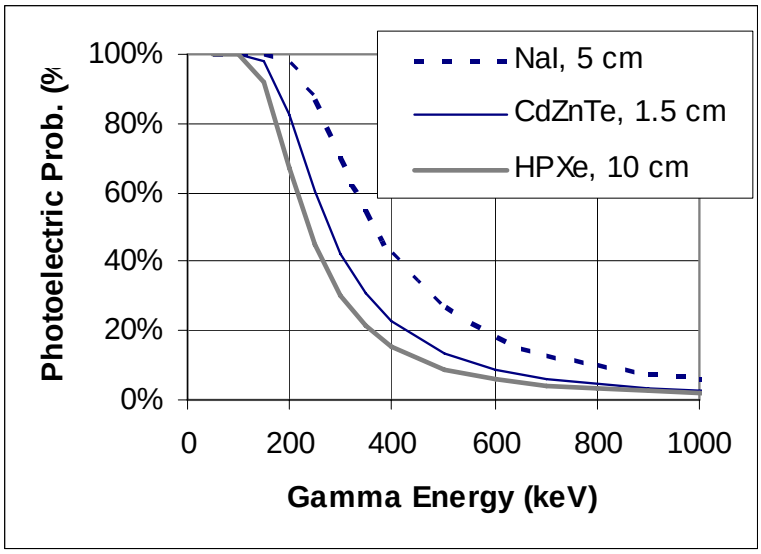

Fig. 17. The intrinsic photoelectric efficiency is plotted vs. gamma-ray energy for a 5-cm-thick compact NaI detector (dashed), the 1.5-cm-thick (largest) CPG CdZnTe detector (light solid line), and 10-cm-diameter HPXe (heavy solid line) detector with gas density of 0.4 g/cm^3.

Fig. 18. Commercial prototype HPXe detector. The diameter and active length are 4.5 and 10 cm.

Figure 19 and Table 1 indicate that the energy resolution of HPXe is similar to that of CdZnTe.[124] However, only HPXe detectors can be scaled up in size for potential applications not available to CdZnTe. All of the benefits of gas detectors apply to the HPXe detectors. Acoustic effects on the grid and electronic effects contribute to limitations in energy resolution. Experimental efforts include investigating alternatives to the grid.[125]

The inherent ruggedness and stability of gas counters is demonstrated by decades of stable operation of He^3 neutron detectors. Equivalent data for HPXe comes from the reliable and stable performance of such a detector monitoring the 511-keV gamma ray during six years of continuous operation on the earth-orbiter MIR.[126] The superior temperature stability of HPXe has been demonstrated with measurements of the 662-keV gamma-ray of ^{137}Cs at different temperatures. Figure 20 is a plot of the energy resolution of the HPXe detector measured at 662 keV as a function of temperature. Also plotted on the graph is the resolution of CdZnTe. The increase in resistivity with increasing temperature of a solid state detector compromises the charge-collection properties, as illustrated in Figure 20. Figure 21 shows the drift in the centroid of the 662-keV peak measured with the HPXe detector as a function of temperature.[127] Comparable data for NaI or other scintillators would show a drift of ~40% in the same temperature range.

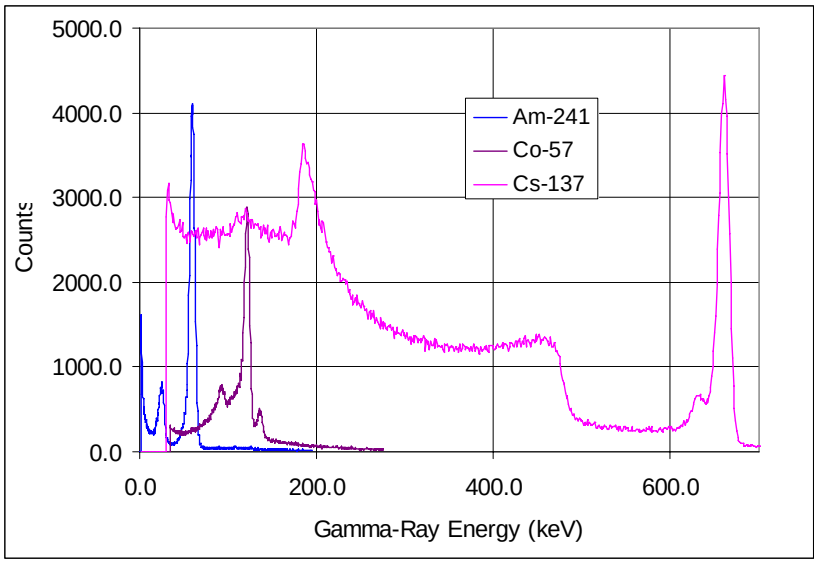

Fig. 19. Gamma-ray spectra of ^{241}Am, ^{57}Co and ^{137}Cs measured with the HPXe detector pictured in Figure 17 indicate energy resolution comparable to that of the CPG CdZnTe detector.

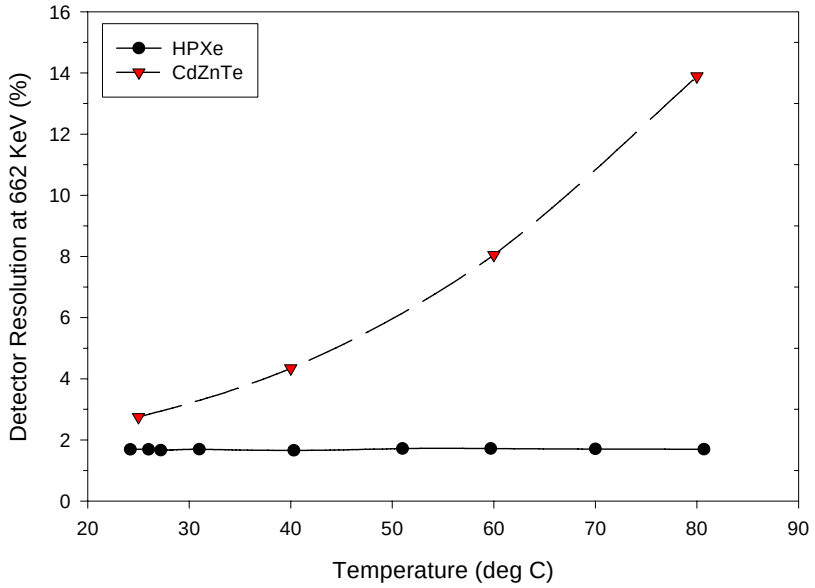

Fig. 20. The resolution (FWHM) at 662 keV of the HPXe detector (circles) and CdZnTe (triangles) is plotted vs. temperature of the detector.

Numerical modeling of the HPXe detector response supports new designs with reduced sensitivity to vibration. Such modeling also supports assessments of novel applications such as the addition of ^{3}He to the high-pressure xenon gas.[128] Figure 22 shows the modeled spectrum for such a detector measuring a ^{137}Cs source and thermal neutrons simultaneously. Other work on electron drift velocities indicates the practical feasibility of spectroscopic measurements of gamma rays and neutron capture using the Xe-^{3}He gas mixture.[129] Such detectors could be most useful for monitoring materials in enrichment facilities, particularly for the processes that operate at high temperature.

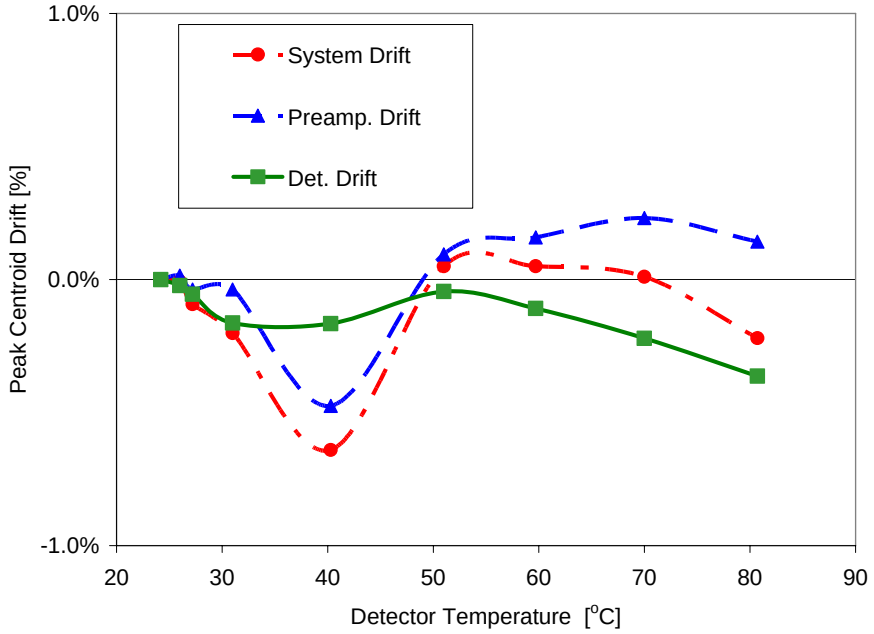

Fig. 21. The percent drift in the 662-keV peak centroid is plotted vs. temperature for the preamplifier (triangles), HPXe detector (squares) and the whole system (circles). Comparable NaI data would show large drifts (40%).

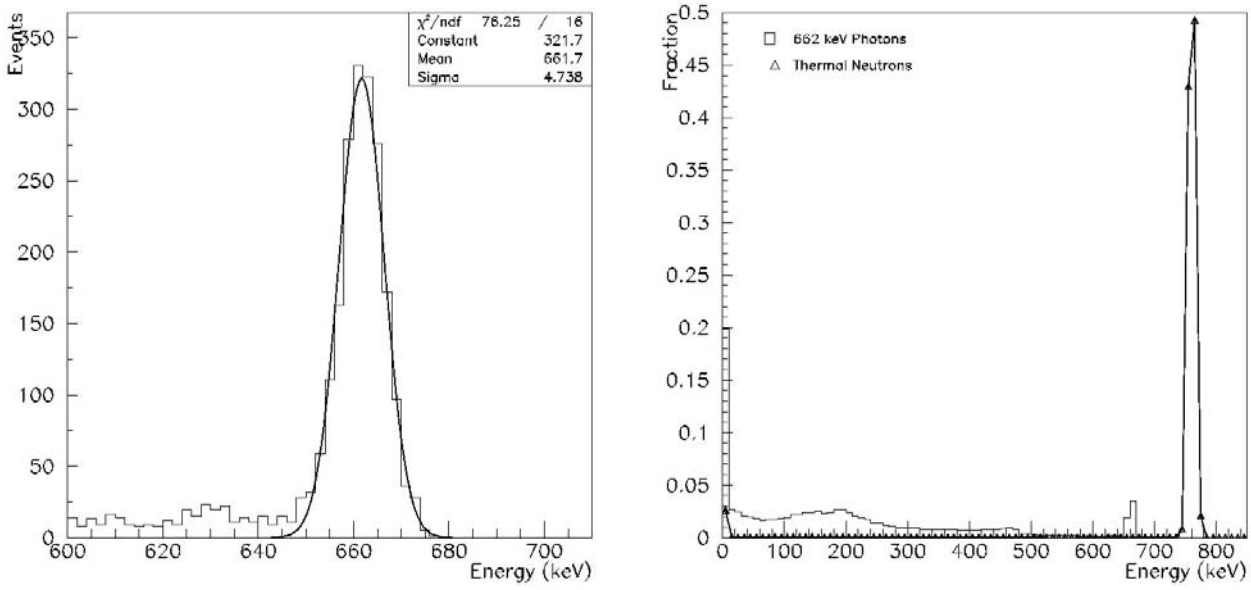

Fig. 22. Simulated pulse-height spectra of ^{137}Cs plus thermal neutrons for the HPXe gas detector with ^{3}He. The 600-700-keV region (left) shows the 662-keV peak with a FWHM of 1.7%, similar to experiment. The full spectrum (right) shows the ^{3}He neutron-capture peak near 750 keV and the ^{137}Cs peak at 662 keV.

The benefits of intermediate energy resolution, ruggedness, resistance to radiation damage, temperature stability far exceeding that of solid-state and scintillator detectors, the ability to scale detectors to large sizes, and the resistance of gas detectors to damaging effects of radiation combine to strongly encourage continued improvement of HPXe detectors for spectroscopy. A practical acoustically desensitized design for the HPXe detector is the promise for continuous unattended monitoring of nuclear materials.

VIII. ORGANIC SCINTILLATORS: PB-LOADED PLASTIC FOR DNS

The ability to create very large scintillators of almost any shape is a characteristic of plastic scintillators, which are used worldwide in portal monitoring of personnel and vehicles. The low cost of plastic scintillators is another benefit. The tendency for personnel and vehicle monitors to alarm from the detection of legitimate radiation (e.g. medical isotopes) far exceeds the alarm rate from detection of illicit radioactive materials, because plastic scintillators have no energy resolution.

The low photoelectric cross-section in low-Z, low-density plastic is the reason that plastic scintillators are not spectrometers. Most gamma rays interact in plastic by Compton scattering and the resulting spectrum is an energy continuum with no peak. However, the loading of plastic scintillators with high-Z materials achieves a dramatic increase in the theoretical photoelectric cross-section. Figure 23 illustrates this increase with theoretical photoelectric and total interaction probabilities of the typical plastic scintillator compared to those with 5% and 10% lead loadings. The results are calculated for three thicknesses of plastic scintillator: 5, 10 and 15 cm. The 5-cm-thick plastic scintillator is used commonly in portal monitors.

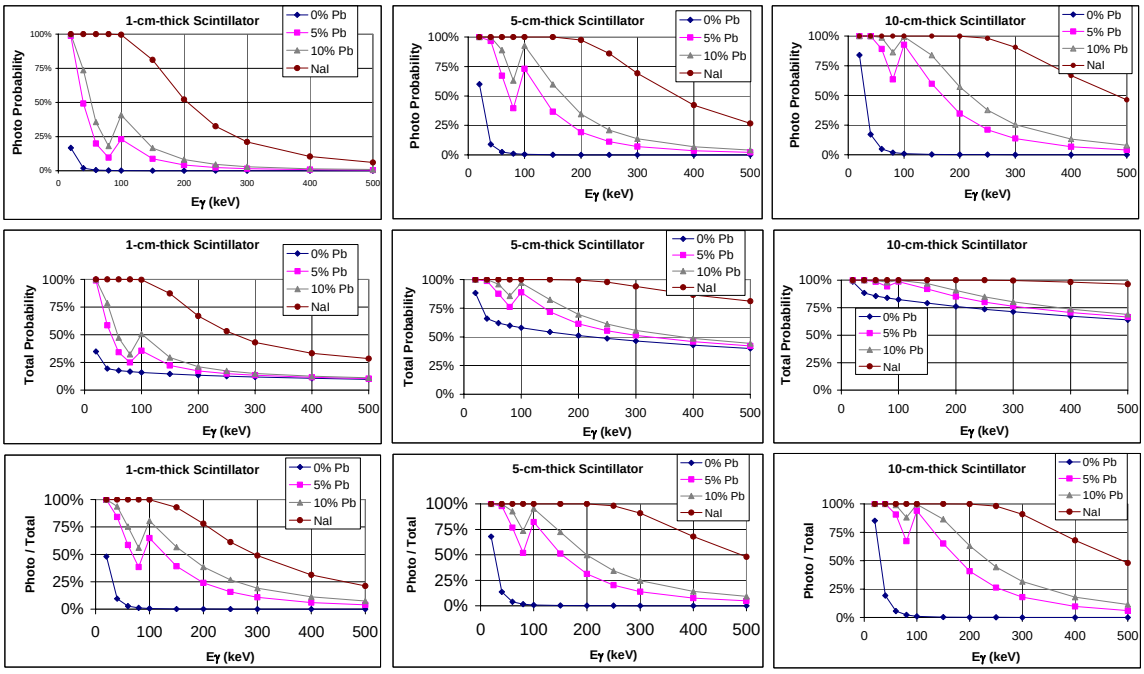

Fig. 23. Theoretical photoelectric and total cross-section (and the ratio of photoelectric to total) of the typical plastic scintillator compared to those with 5% and 10% lead loadings of lead by weight are plotted vs. gamma-ray energy. The results are calculated for three thicknesses of plastic scintillator: 5, 10 and 15 cm. Also plotted for reference are the corresponding data for the NaI scintillator of the same thickness.

Experimental data provide compelling evidence of the spectroscopic capability of lead-loaded plastic scintillators, corroborating the theoretical results in Figure 23. Gamma-ray spectra of ^{109}Cd, ^{57}Co and ^{235}U were measured using a small disk (5-cm-diameter by 1.27-cm-thick) of 5%-lead-

loaded commercial plastic scintillator coupled to a 6.5-cm-diameter photomultiplier tube. The small scintillator piece is clear and colorless and has no apparent flaws to limit light transmission. Figure 24 illustrates the experimental setup with two source positions. Evidence of spectroscopic capability is most apparent with the sources in Position 2, in which some gamma-ray path lengths in the were as long as 5 cm. Figure 25 shows the three gamma-ray spectra measured with the lead-loaded plastic. The energy calibration, gamma-ray-peak energy vs. channel number, in the inset, is linear. The energy resolution at 122 keV (the ^{57}Co is 23%, about twice that of NaI at this energy.[130]

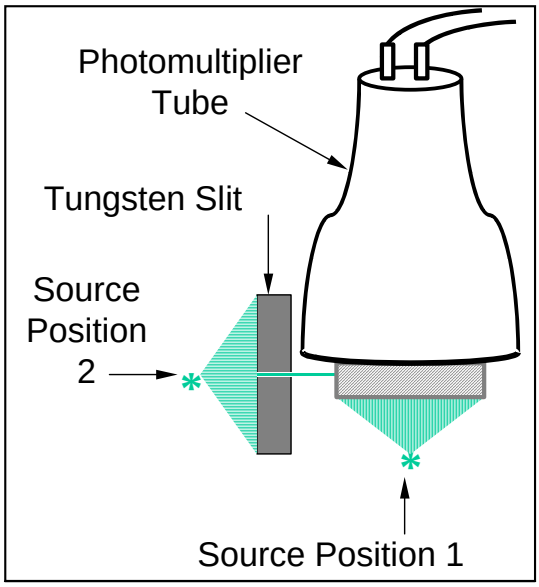

Fig. 24. Hardware setup for measurements of gamma-ray spectra with the 5%-lead-loaded plastic scintillator (diagonally shaded) coupled to a photomultiplier tube. The1.3-cm-thick tungsten collimator is a 5-cm-wide by2-mm-tall horizontal slit.

The 186-keV gamma-ray peak is only partly resolved in the spectrum shown in Figure 25. A higher lead loading should significantly enhance the definition of this peak relative to the continuum, as indicated by the data in Figure 23. Figure 23 also suggests that spectroscopy at higher gamma-ray energies such as 414-keV (^{239}Pu) may not be practical for any of the high-Z-loaded plastics. However, applications to ^{235}U in continuous measurements using distributed networked scintillators should be practical. Unlike portable measurements in which the best possible resolution must combine with a robust analysis algorithm, the algorithms used for each fixed sensor can be tailored to the much smaller range of variations at each fixed location.

The quality of the small commercial 5%-lead-loaded plastic scintillator used to obtain the spectra plotted in Figure 25 is extremely good from the standpoint of clarity and absence of color. Despite momentum provided by the encouraging results obtained with this scintillator, commercial manufacturers have achieved no progress toward production of practical scintillator pieces of larger size or higher lead loadings. Because the potential benefit to portal monitoring and DNS is so great, efforts continue to develop the lead-loaded plastic scintillator materials for these applications.

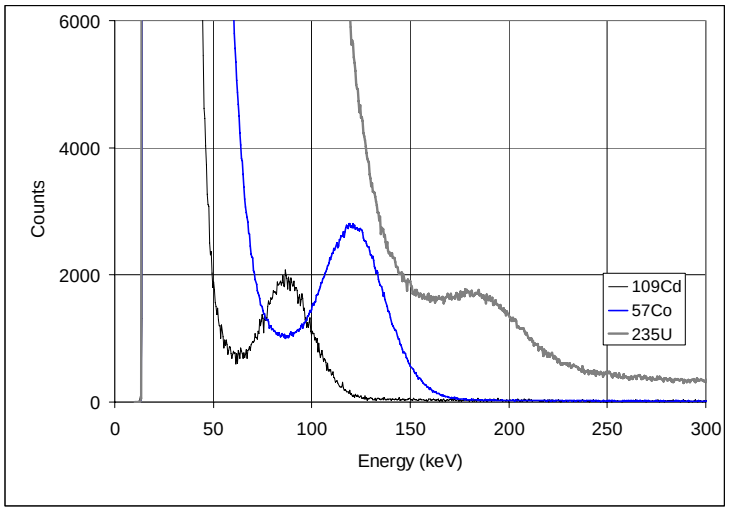

Fig. 25. Pulse-height spectra for three gamma-ray source, ^{109}Cd, ^{57}Co and ^{235}U, in source position 2 (see Figure 22). The energies of the three photopeaks (88, 122 and 186 keV) plotted vs. peak channel in the inset illustrate the linearity of the pulse amplitude with energy.

Another very new approach with plastics serving as host is one which embeds nanoparticles of an active sensor, either semiconductor[131] or inorganic scintillator,[132] in a solid organic – sometimes scintillating – matrix. Growth of large crystals with ideal properties for transporting charge (semiconductor materials) or light (inorganic scintillators) is replaced, in the cases of these new detectors, with production of nanoparticulates[133] of the same material. The organic matrix governs the transport and determines the overall detector geometry while the properties of the nanoparticulates determine performance. The potential includes very large spectrometer detectors, improved resolution, and low cost.

END NOTES

[1] D. Reilly, et. al., *Passive Nondestructive Assay of Nuclear Materials,* 1991, pp. 43-64.
[2] P. A. Russo, 2005.
[3] P. A. Russo, T. R. Wenz, and K. D. Veal, 2000.
[4] V. Longmire, N. Ensslin, C. Files *et al*., 2004.
[5] G. F. Knoll, 2000, pp. 231-242.
[6] G. F. Knoll, 2000, pp. 265-287.
[7] P. A. Russo, T. R. Wenz, and J. A. Painter, 1992.
[8] T. Ludziejewski, K. Moszynska, M. Moszynski, *et al*., 1995.
[9] A. Romano and P. Russo, 1999.
[10] P. Dorenbos, 2002.
[11] P. Dorenbos, J. T. M. de Haas, and C. W. E. van Eijk, 2004.
[12] K. S. Shah, J. Glodo, M. Klugerman, *et al*., 2003.
[13] E. V. D. van Loef, P. Dorenbos, C. W. E. van Eijk, *et al*., 2000.
[14] E. V. D. van Loef, P. Dorenbos, C. W. E. van Eijk, *et al*., 2001.
[15] E. V. D. van Loef, W. Mengesha, J. D. Valentine, *et al*., 2003.
[16] A. Kh. Khusainov, J. S. Iwanczyk, B. E. Patt, *et al*., 2001.
[17] D. T. Vo and P. A. Russo, 2002.
[18] D. T. Vo and P. A. Russo, *Nucl. Instr. Meth.,* 2002.
[19] D. T. Vo and P. A. Russo, 2004.
[20] P. N. Luke and E. E. Eissler, 1996.
[21] Z. He, G. F. Knoll, D. K. Wehe, *et al*., 1996.
[22] T. H. Prettyman, M. K. Smith and S. E. Soldner, 1999.
[23] T. H. Prettyman, M. C. Browne, K. D. Ianakiev, *et al*., 2000.
[24] R. Redus, A. Huber, J. Pantazis, *et al.*, 2004.
[25] D. T. Vo, P. A. Russo, and T. E. Sampson, 1998.
[26] D. T. Vo, August 1999.
[27] D. T. Vo, November 1999.
[28] D. T. Vo and P. A. Russo, February 2002.
[29] C. Frankle, 2003.
[30] K. P. Ziock, W. W. Craig, L. Fabris, *et al*., 2004.
[31] D. Cordle, J. Gross, and B. McGinnis, 2000.
[32] D. H. Beddingfield, A. P. Belian, K. D. Veal, *et al.*, 2003.
[33] G. J. Schmid, D. A. Beckedahl, J. E. Kaameraad, *et al.*, 2001.
[34] K. Vetter, M. Burks, and L. Mihailescu, 2004.
[35] C. E. Lehner, Z. He, and F. Zhang, 2004.
[36] M. Amman and P. N. Luke, 2000.
[37] W. Coburn, S. Amrose, S. E. Boggs, *et al.,* 2002.
[38] K. Vetter, L. Mihailescu, K. Ziock, *et al.,* 2002.
[39] J. Y. Huang and D. T. Vo, 2004.
[40] K. Chung, A. P. Belian, E. A. McKigney, and P. A. Russo, 2004.
[41] A. Bolotnikov and B. Ramsey. *Nucl. Instr. Meth*.,1997.
[42] V. V. Dmitrenko, V. M. Gratchev, S. E. Ulin, *et al.*, 2000.
[43] S. Kobayashi, V. V. Dmitrenko, T. Doke, *et al.*, 2003.
[44] C. Levin, J. Germani, and J. Markey, 1993.
[45] G. J. Mahler, B. Yu, B.; G. C. Smith, *et al.*, 1998.
[46] E. A. McKigney and M. K. Smith, 2004.
[47] D. H. Beddingfield, A. Beyerle, P. A. Russo, *et al*., 2003.

[48] S. E. Ulin, K. F. Vlasik, A. M. Galper, *et al.*, 1997.
[49] D. Reilly, et. al., *Passive Nondestructive Assay of Nuclear Materials*, 1991, pp. 43-64.
[50] G. F. Knoll, 2000, pp. 231-287.
[51] G. F. Knoll, 2000, p. 235.
[52] G. F. Knoll, 2000, pp. 231-260.
[53] G. F. Knoll, 2000, p. 233.
[54] K. D. Ianakiev, M. Abhold, B. Alexandrov, *et al.*, 2005.
[55] F. E. Fenimore and T. M. Cannon, 1978.
[56] K. P. Ziock, W. W. Craig, L. Fabris, *et al*., 2004.
[57] D. H. Beddingfield, A. P. Belian, K. D. Veal, *et al.*, 2003.
[58] D. Cordle, J. Gross, and B. McGinnis, 2003.
[59] K. P. Ziock, M. T. Burks, W. Craig, *et al.*, 2003.
[60] P. A. Russo, 2005.
[61] R. Gunnink, R. Arlt, and R. Berndt, 1997.
[62] P. A. Russo, 2005.
[63] A. P. Belian, T. D. Reilly, P. A. Russo, *et al.*, 2005.
[64] G. F. Knoll, 2000, pp. 287-300.
[65] Y. J. Wang, B. E. Patt, J. S. Iwanczyk, *et al.*, 1996.
[66] K. S. Shah, R. Farrell, R. Grazioso, *et al.*, 2002.
[67] M. Moszynski, W. Czarnacki, W. Klamra, *et al*., 2003.
[68] G. F. Knoll, 2000, pp. 297-300.
[69] A. P. Belian, K. D. Ianakiev, and P. A. Russo, 2001.
[70] G. F. Knoll, 2000, pp. 239-240.
[71] D. W. Cooke, B. L. Bennett, K. J. McClellan, *et al.*, 2002.
[72] P. Dorenbos, J. T. M. de Haas, and C. W. E. van Eijk,, 2004.
[73] E. V. D. van Loef, W. Mengesha, J. D. Valentine, *et al.*, 2003.
[74] D. W. Cooke, B. L. Bennett, K. J. McClellan, *et al.*, 2002.
[75] T. Ludziejewski, K. Moszynska, M. Moszynski, *et al.*, 1995.
[76] K. Chung, A. P. Belian, E. A. McKigney, and P. A. Russo, 2004.
[77] P. Dorenbos, J. T. M. de Haas, and C. W. E. van Eijk,, 2004.
[78] K. Chung, A. P. Belian, E. A. McKigney, and P. A. Russo, 2004.
[79] *Ibid.*
[80] D. Reilly, et. al., *Passive Nondestructive Assay of Nuclear Materials*,1991, pp. 43-64.
[81] D. T. Vo, 2005.
[82] D. T. Vo and P. A. Russo, *Nucl. Instr. Meth*., 2002.
[83] D. T. Vo and P. A. Russo, 2004.
[84] C. Frankle, 2003.
[85] S. Friedrich, S. F. Terracol, T. Miyazaki, *et al.*, 2004.
[86] O. B. Drury, S. F. Terracol, and S. Friedrich, 2005.
[87] M. W. Rabin, C. R. Rudy, M. K. Smith, *et al.*, 2005.
[88] J. N. Ullom, J. A. Beall, W. B. Doriese, *et al.*, 2005.
[89] D. T. Vo, P. A. Russo, and T. E. Sampson, 1998.
[90] D. T. Vo and P. A. Russo, February 2002.
[91] G. F. Knoll, 2000, p. 628.
[92] D. T. Vo, August 1999.
[93] K. P. Ziock, M. T. Burks, W. Craig, *et al.*, 2003.
[94] G. J. Schmid, D. A. Beckedahl, J. E. Kaameraad, *et al.*, 2001.
[95] K. Vetter, M. Burks, and L. Mihailescu, 2004.
[96] C. E. Lehner, Z. He, and F. Zhang, 2004.
[97] M. Amman and P. N. Luke, 2000.

[98] W. Coburn, S. Amrose, S. E. Boggs, *et al.,* 2002.
[99] K. Vetter, L. Mihailescu, K. Ziock, *et al*., 2002.
[100] G. F. Knoll, 2000, pp. 477-488.
[101] G. F. Knoll, 2000, pp. 358-359.
[102] C. Szeles, S. E. Cameron, S. A. Soldner, *et al.*, 2004.
[103] P. N. Luke, 1994 and 1996.
[104] P. N. Luke and E. E. Eissler, 1996.
[105] Z. He, G. F. Knoll, D. K. Wehe, *et al*., 1996.
[106] T. H. Prettyman, M. C. Browne, K. D. Ianakiev, *et al*., 2000.
[107] C. E. Lehner, Z. He, and F. Zhang, 2004.
[108] C. Szeles, S. E. Cameron, S. A. Soldner, *et al.*, 2004.
[109] P. N. Luke, 1994 and 1996.
[110] P. N. Luke and E. E. Eissler, 1996.
[111] Z. He, G. F. Knoll, D. K. Wehe, *et al*., 1996.
[112] C. E. Lehner, Z. He, and F. Zhang, 2004.
[113] M. Rawool-Sullivan, W. Murray, K. Kreuger, and L. Ussery, 1997.
[114] P. A. Russo, A. P. Meier, M. Rawool-Sullivan, *et al.*, 1997.
[115] P. A. Russo, T. H. Prettyman, S. E. Smith, *et al.*, 1999.
[116] D. T. Vo, P. A. Russo, and S. A. Soldner, 1999.
[117] J. Y. Huang, and D. T. Vo, 2004.
[118] A. Kh. Khusainov, J. S. Iwanczyk, B. E. Patt, *et al*., 2001.
[119] D. T. Vo and P. A. Russo, *Nucl. Instr. Meth.,* 2002.
[120] D. T. Vo and P. A. Russo, 2004.
[121] R. Redus, A. Huber, J. Pantazis, *et al.*, 2004.
[122] G. F. Knoll, 2000, pp. 716-717.
[123] G. F. Knoll, 2000, p. 152.
[124] D. H. Beddingfield, A. Beyerle, P. A. Russo, *et al*., 2003.
[125] C. J. Sullivan, Z. He, G. F. Knoll, *et al.*, 2003.
[126] S. E. Ulin, K. F. Vlasik, A. M. Galper, *et al.*, 1997.
[127] D. H. Beddingfield, A. Beyerle, P. A. Russo, *et al*., 2003.
[128] E. A. McKigney and M. K. Smith, 2004.
[129] S. Kobayashi, V. V. Dmitrenko, T. Doke, *et. al.*, 2003.
[130] K. Chung, A. P. Belian, E. A. McKigney, and P. A. Russo, 2004.
[131] I. H. Campbell, and B. K. Krone, 2005.
[132] D. W. Cooke, J.-K. Lee, B. L. Bennett, *et al.*, 2005.
[133] W. Zhang, P. Xie, C. Duan, *et al.*, 1998.

REFERENCES

Amman, M., and P. N. Luke, "Three-Dimensional Position Sensing and Field Shaping in Orthogonal-Strip Germanium Gamma-Ray Detectors," *Nucl. Instr. Meth*. A 452 (2000), pp. 155-166.

Beddingfield, D. H., A. P. Belian, K. D. Veal, P. A. Russo, V. Longmire, V. A. Hatler, C. L. Kowalczyk, and M. K. Romero, "Measuring In-Process Inventory by Spectroscopic Imaging," Los Alamos National Laboratory report LA-UR-03-4066, 2003. *Proceedings of 44th Annual Meeting of the INMM*, CD ROM, Northbrook IL: INMM (2003).

Beddingfield, D. H., A. Beyerle, P. A. Russo, K. Ianakiev, D. T. Vo, and V. Dmitrenko, "High-Pressure Xenon Ion Chambers for Gamma-Ray Spectroscopy in Nuclear Safeguards," *Nucl. Instr. Meth.* A 505 (2003), pp. 474-477.

Belian, A. P., K. D. Ianakiev, and P. A. Russo, "Measuring the Number of Photoelectrons from Neutron Capture Events In a LiF/ZnS Scintillator/Fiber Optic Neutron Detector," Los Alamos National Laboratory report LA-UR-01-1818 (2001).

Belian, A. P, T. D. Reilly, P. A. Russo, S. J. Tobin, N. N. Nikolaenko, G. Sokolov, Y. V. Yasko, A. Ustimovich, G. Strygin, Y. Tchyrnuha, A. Chahid, A. LeBrun, and L. Bourva, "Holdup Measurements at the Ulba Metallurgical Plant," Los Alamos National Laboratory report LA-UR-05-2020 (March 2005).

Bolotnikov, A., and B. Ramsey. "The Spectroscopic Properties of High-pressure Xenon," *Nucl. Instr. Meth*. A 396 (1997), pp. 360-370.

Campbell, I. H., and B. K. Krone, "Quantum Dot/Organic Semiconductor Composites for Radiation Detection," Los Alamos National Laboratory report LA-UR-05-2578. (Submitted to *Applied Physics Letters*.)

Chung K., A. P. Belian, E. A. McKigney, and P. A. Russo, "Application of Lanthanum Halide Scintillators and Low-Resolution Dense Plastics for Modern MC&A Needs," Los Alamos National Laboratory report LA-UR-04-4472, 2004. *Proceedings of 45th Annual Meeting of the INMM*, CD ROM, Northbrook IL: INMM (2004).

Coburn, W., S. Amrose, S. E. Boggs, R. P. Lin, M. Amman, M. T. Burks, E. L. Hull, P. N. Luke and N. Madden, "3-D Positioning Germanium Detectors for Gamma-Ray Astronomy," *SPIE* 4784 (2002), pp. 54-63.

Cooke, D. W., B. L. Bennett, K. J. McClellan, R. E. Muenchausen, J. R. Tesmer, and C. J. Wetteland, "Luminescence, Emission Spectra, and Hydrogen Content of Crystalline $Lu_2SiO_5:Ce^{3+}$," *Philosophical Magazine* B 82, No. 2 (2002), pp. 1659-1670.

Cooke, D. W., J.-K. Lee, B. L. Bennett, J. R. Groves, R. E. Muenchausen, M. Nastasi, K. E. Sickafus, M. Tang, and J. A. Valdez, "Optical Properties of Hydrothermally Prepared Y2SiO5:Ce Nanophosphors," Los Alamos National Laboratory report LA-UR-05-____. (Submitted to *Applied Physics Letters*.)

Cordle, D., J. Gross, and B. McGinnis, "Gamma-Ray Imaging for Qualitative Uranium Material Holdup Position Determination and Improved Quantitative Mass Determination," United States Enrichment Corporation report, 2000. *Proceedings of the 41st Annual Meeting of the INMM*, CD ROM, Northbrook IL: INMM (2000).

Dorenbos, P., "Light Output and Energy Resolution of Ce^{3+}-Doped Scintillators," *Nucl. Instr. Meth*. A 486 (2002), pp. 208-213.

Dorenbos, P., J. T. M. de Haas, and C. W. E. van Eijk, "Gamma Ray Spectroscopy With a ∅ 19 × 19 mm^3 $LaBr_3$: 0.5% Ce^{3+} Scintillator," *IEEE Trans. Nucl. Sci.* 51, (2004), pp. 1289-1296.

Dmitrenko, V. V., V. M. Gratchev, S. E. Ulin, Z. M. Uteshev, K. F. Vlasik, "High Pressure Xenon Detectors for Gamma-ray Spectroscopy." *Appl. Rad. Iso*. 52 (2000), pp. 739-743.

Drury, O. B., S. F. Terracol, and S. Friedrich, "Quantifying the Benefits of Ultrahigh Energy Resolution for Gamma-Ray Spectrometry." *Phys. Stat. Sol.* (C) 2 (2005), pp. 1468-1479.

Fenimore, F. E., and T. M. Cannon, "Coded-Aperture Imaging with Uniformly Redundant Arrays," *Applied Optics* Vol. 17, No. 3 (1978), pp. 337-347.

Frankle, C., Los Alamos National Laboratory, private communication of information contained in patent application S-99,935 ("Handheld Isotope Identification System") 2003.

Friedrich, S., S. F. Terracol, T. Miyazaki, O. B. Drury, Z. A. Ali, M. F. Cunningham, T. R. Niedermayr, T. W. Barbee Jr., J. D. Batteux, and S. E. Labov, "Design of a Multichannel Ultra-High Resolution Superconducting Gamma-Ray Spectrometer," *SPIE* 5540 (2004), pp. 156-164.

Gunnink, R., R. Arlt, and R. Berndt, "New Ge and NaI Analysis Methods for Measuring 235U Enrichments," *Proceedings of the 19th ESARDA Meeting*, Montpellier, France (May, 1997), pp. 431-435.

He, Z., G. F. Knoll, D. K. Wehe, R. Rojeski, C. H. Mastrangelo, M. Hammig, C. Barrett and A. Uritani, "1-D Position Sensitive Single Carrier Semiconductor Detectors," *Nucl. Instr. Meth*. A 380 (1996), pp. 228-231.

Huang, J. Y., and D. T. Vo, "Distributed Miniature Radiation Detectors for Monitoring Plutonium Casting Processes," Los Alamos National Laboratory report LA-UR-04-4449, 2004. (*Proceedings of the Institute of Nuclear Materials Management*, 45th Annual Meeting, Orlando, FL, July 18-22, 2004, CD ROM.)

Ianakiev, K. D., M. Abhold, B. Alexandrov, J. Audia, M. C. Browne and H. Nguyen, "Temperature Behavior of Doped NaI(Tl) Scintillators and Its Impact on Pulse Height Analysis Instrumentation." Los Alamos National Laboratory report LA-UR-05-3409. (Submitted for presentation at the 2005 IEEE NSS/MIC Conference, San Juan USA, October 23-29, 2005.)

Khusainov, A. Kh., J. S. Iwanczyk, B. E. Patt, A. M. Pirogov, D. T. Vo and P. A. Russo, "Approaching Cryogenic Ge Performance with Peltier Cooled CdTe," Los Alamos National Laboratory report LA-UR-01-4123 (2001). *SPIE* 4507 (2001), pp. 50-56.

Knoll, G. F., *Radiation Detection and Measurement*, Third Edition (John Wiley and Sons, Inc., New York, 2000).

Kobayashi, S., V. V. Dmitrenko, T. Doke, V. M. Grachev, N. Hasebe, T. Igarashi, T. Miyachi, H. Okada, E. Shibamura, M. Takenouchi, S. E. Ulin, and K. F. Vlasik, "Measurement of Electron Drift Velocities in the Mixture of Xe and He for a New High-Pressure Xe Gamma-Ray Detector," *Japan. J. App. Phys*. 42:1 (2003), pp. 333-334.

Lehner, C. E., Z. He, and F. Zhang, "4-π Compton Imaging Using a 3-D Position-Sensitive CdZnTe Detector Via Weighted List-Mode Maximum Likelihood," *IEEE Trans. Nucl. Sci*. 51 (2004), pp. 1618-1624.

Levin,C., J. Germani, and J. Markey, "Charge Collection and Energy Resolution Studies in Compressed Xenon Gas near its Critical Point," *Nucl. Instr. Meth*. A 332 (1993), pp. 206-214.

Longmire, V., N. Ensslin, C. Files, J. Joseph, C. Rudy, M. Smith, P. Russo, R. Stevens, R. Strittmatter, D. Wilkey, C. Pickett, W. Brosey, and J. Swanson, "The SO-20.3 MC&A Modernization Plan," Version I, Los Alamos National Laboratory controlled paper LA-CP-04-0235 (April 9, 2004).

Ludziejewski, T., K. Moszynska, M. Moszynski, D. Wolski, W. Klamra, L.O. Norlin, E. Devitsin, and V. Kozlov, "Advantages and Limitations of LSO Scintillator in Nuclear Physics Experiments," *Trans. Nucl. Sci.* 42 (1995), pp. 328-336.

Luke, P. N., "Single-Polarity Charge Sensing in Ionization Detectors Using Coplanar Electrodes," *Appl. Phys. Lett*. 65 (1994), pp. 2884-2886.

Luke, P. N., "Electrode Configuration and Energy Resolution in Gamma-ray Detectors," *Nucl. Instr. Meth*. A 380 (1996), pp. 232-237.

Luke, P. N., and E. E. Eissler, "Performance of CdZnTe Coplanar-Grid Gamma-Ray Detectors," *IEEE Trans. Nucl. Sci*. 43 (1996), pp. 1481-1486.

Mahler, G. J., B. Yu, B.; G. C. Smith, W. Kane, and J. R. Lemley, "A Portable Gamma-ray Spectrometer Using Compressed Xenon," *IEEE Trans. Nucl. Sci*. 45 (1998), pp. 1029-1033.

McKigney, E. A., and M. K. Smith, "Simulation of a High-Pressure Xe-3He Detector" Los Alamos National Laboratory report LA-UR-04-4359, 2004. (*Proceedings of the Institute of Nuclear Materials Management*, 45th Annual Meeting, Orlando, FL, July 18-22, 2004, CD ROM.)

Moszynski, M. W. Czarnacki, W. Klamra, M. Szawlawski, P. Schotanus, and M. Kapusta, "Intrinsic Energy Resolution of Pure NaI Studied with Large Area Avalanche Photodiodes at Liquid Nitrogen Temperatures," *Nucl Instr. Meth*. A 505 (2003), pp. 63-67.

Passive Nondestructive Assay of Nuclear Materials. D. Reilly, N. Ensslin, H. Smith, Jr., eds. (Nuclear Regulatory Commission NUREG/CR-5550, 1991), Los Alamos National Laboratory report LA-UR-90-732 (1990).

Prettyman, T. H., M. K. Smith and S. E. Soldner, "Design and Characterization of Cylindrical CdZnTe Detectors with Coplanar Grids," *SPIE 3768* (1999) 339-345.

Prettyman, T. H., M. C. Browne, K. D. Ianakiev, C. E. Moss, S. E. Soldner, "Characterization of a Large-Volume Multi-Element CdZnTe Detector," *SPIE 4141* (2000), pp. 1-10.

Rabin, M. W., C. R. Rudy, M. K. Smith, D. M. Tournear, and D. T. Vo, J. N. Ullom, and K. D. Irwin, "Nuclear Applications of Large Arrays of High-Resolution Microcalorimeters," Los Alamos National Laboratory report LA-UR-05-3431. (Submitted for presentation at the 2005 IEEE NSS/MIC Conference, San Juan USA, October 23-29, 2005.)

Rawool-Sullivan, M., W. Murray, K. Kreuger, and L. Ussery, "CdZnTe Progress Report for June 1997," Los Alamos National Laboratory report LA-UR-97-2900, 1997.

Redus, R., A. Huber, J. Pantazis, T. Pantazis, T. Takahashi and S. Woolf, "Multielement CdTe Stack Detectors for Gamma-Ray Spectroscopy," *IEEE Trans. Nucl. Sci*. 51 (2004), pp. 2386-2394.

Reilly, D., Ensslin, N., and Smith, H., Passive Nondestructive Assay of Nuclear Materials, Nuclear Regulatory Commission report NUREG/CR-5550, Los Alamos National Laboratory report LA-UR-90-732 (March 1991).

Romano, A., and P. Russo, "Investigating the Use of Lu(SiO4)O:Ce for Gamma-Ray Spectroscopy," Los Alamos National Laboratory report LA-UR-99-4332 (1999).

Russo, P. A., T. R. Wenz, and J. A. Painter, "Experimental Evaluation of Software-Driven Digital Gain-Drift Compensation in Scintillator Gamma-Ray Spectroscopy," Los Alamos National Laboratory report LA-12390-MS (1992).

Russo, P. A., A. P. Meier, M. Rawool-Sullivan, T. H. Prettyman, H. Y. Huang, D. A. Close, M. C. Sumner, R. A. Cole, P. N. Luke and S. A. Soldner, "A New Room-Temperature Gamma-Ray Detector for Improved Assay of Plutonium," Los Alamos National Laboratory report LA-UR-97-2782, 1997. (*Proceedings of the Institute of Nuclear Materials Management*, 38th Annual Meeting, Phoenix AZ, July 20-24, 1997, CD ROM.)

Russo, P. A., T. H. Prettyman, S. E. Smith, J. F. Harris, J. S. Massengill and E. Stair, Jr., "Comparison of Detectors for Portable Gamma-Ray Spectroscopy at Y-12," Los Alamos National Laboratory report LA-UR-99-199 (January 1999).

Russo, P. A., T. R. Wenz, and K. D. Veal, "In-Situ Measurement of Process Solution Inventory of ^{235}U," Los Alamos National Laboratory report LA-UR-00-2470 (June 2000).

Russo, P. A., "Gamma-ray Measurements of Holdup Plant-wide: Application Guide for Portable Generalized Approach", Los Alamos report LA-14206 (March 2005).

Schmid, G. J., D. A. Beckedahl, J. E. Kaameraad, J. J. Blair, K. Vetter, and A. Kuhn, Gamma-Ray Compton Camera Imaging with a Segmented HPGe," *Nucl. Instr. Meth*. A 459(2001), pp. 565-576.

Shah, K. S., R. Farrell, R. Grazioso, E. S. Harmon, and E. Karplus," Position-Sensitive Avalanche Photodiodes for Gamma-Ray Imaging," *IEEE Trans. Nucl. Sci*. 49 (2002), pp. 1687-1692.

Shah, K. S., J. Glodo, M. Klugerman, L. Cirignano, W. W. Moses, S. E. Derenzo, M. J. Weber, "$LaCl_3$:Ce Scintillator for Gamma-ray Detection," *Nucl. Instr. Meth*. A 505(2003), pp. 76-81.

Sullivan, C. J., Z. He, G. F. Knoll, G. B. Tepper, and D. K. Wehe, "A High Pressure Xenon Gamma-ray Spectrometer Using a Coplanar Anode Configuration," *Nucl Instr. Meth*. A 505 (2003), pp. 238-241.

Szeles, C., S. E. Cameron, S. A. Soldner, J. O. Ndap, and M. D. Reed, "Development of the High-Pressure Electrodynamic-Gradient Crystal-Growth Technology of Semi-Insulating CdZnTe for Radiation Detector Applications," *SPIE* 5198 (2004), pp. 191-199. [*Journal of Electronic Materials* 33, No. 6 (2004) 742-751.]

Ulin, S. E., K. F. Vlasik, A. M. Galper, V. M. Grachev, V. V. Dmitrenko, V. I. Liagushin, Z. M. Uteshev, and Yu. T. Yurkin, "Influence of Proton and Neutron Fluxes on Spectrometric Characteristics of a High-pressure Xenon Gamma Spectrometer," *SPIE* 3114 (1997), pp. 499-504.

Ullom, J. N., J. A. Beall, W. B. Doriese, W. D. Duncan, L. Ferreira, G. C. Hilton, K. D. Irwin, C. D. Reintsema, L. R. Vale, B. L. Zink, M. W. Rabin, C. R. Rudy, M. K. Smith, D. M. Tournear, and D. T. Vo, "Development of Large Arrays of Microcalorimeters for Precision Gamma-ray Spectroscopy," NIST Boulder Laboratories report. (Submitted for presentation at the 2005 IEEE NSS/MIC Conference, San Juan USA, October 23-29, 2005.)

van Loef, E. V. D., P. Dorenbos, C. W. E. van Eijk, K. Kramer, and H. U. Gudel, "High-energy-resolution Scintillator: Ce^{3+} Activated $LaCl_{3,}$" *App. Phys. Lett*. 77 (2000), pp. 1467-1468.

van Loef, E. V. D., P. Dorenbos, C. W. E. van Eijk, K. Kramer, and H. U. Gudel, "High-energy-resolution Scintillator: Ce^{3+} Activated $LaBr_{3,}$" *App. Phys. Lett*. 79 (2001), pp. 1573-1575.

van Loef, E. V. D., W. Mengesha, J. D. Valentine, P. Dorenbos, and C. W. E. van Eijk, "Non-proportionality and energy Resolution of a $LaCl_3$:10% Ce^{3+} Scintillation Crystal," *IEEE Trans. Nucl. Sci*. 50 (2003), pp. 155-158.

Vetter, K., L. Mihailescu, K. Ziock, M. Burns, C. Cork, L. Fabris, E. Hull, N. Madden and R. Pehl, "Employing Thin HPGe Detectors for Gamma-Ray Imaging," *Unattended Radiation Sensor Systems for Remote Applications*, AIP 0-7354-0087-3/02 (2002), pp. 129-133.

Vetter, K., M. Burks, and L. Mihailescu, "Gamma-Ray Imaging With Position-Sensitive HPGe Detectors," *Nucl. Instr. Meth*. A 525 (2004), pp. 322-327.

Vo, D. T., P. A. Russo, and T. E. Sampson, "Comparisons Between Digital Gamma-Ray Spectrometer (DSPec) and Standard Nuclear Instrumentation Methods (NIM) Systems," Los Alamos National Laboratory report LA-13393-MS, March 1998.

Vo, D. T., "Evaluations of the Commercial Spectrometer Systems for Safeguards Applications," Los Alamos National Laboratory report LA-13604-MS, August 1999.

Vo, D. T., "Comparisons of the DSPEC and DSPEC Plus Spectrometer Systems," Los Alamos National Laboratory report LA-13671-MS, November 1999.

Vo, D. T., P. A. Russo, and S. A. Soldner, "Experimental Investigation of the Spectroscopic Performance of the Coaxial CdZnTe Detector," Los Alamos National Laboratory report LA-UR-99-580, 1999.

Vo, D. T., and P. A. Russo, "Comparisons of the Portable Digital Spectrometer Systems," Los Alamos National Laboratory report LA-13895-MS, February 2002.

Vo, D. T., and P. A. Russo, "PC/FRAM Plutonium Isotopic Analysis of CdTe Gamma-Ray Spectra," *Nucl. Instr. Meth*. A 486 (2002), pp. 813-824.

Vo, D. T., and P. A. Russo, “Plutonium and Uranium Isotopic Analysis in the X-ray Region with the CdTe Detector,” Los Alamos National Laboratory report LA-UR-03-4730. *SPIE* 5198 (2004), pp. 182-190.

Vo, D. T., “Testing the Detective Systems,” Los Alamos National Laboratory report LA-UR-05-3156, April 2005.

Wang, Y. J., B. E. Patt, J. S. Iwanczyk, S. R. Cherry, and Y. Shao, “Detector Optimization for Handheld CsI:Tl/HgI2 Gamma-ray Scintillation Spectrometer Applications,” ,” *IEEE Trans. Nucl. Sci*. 43 (1996), pp. 1277-1281.

Zhang, W., P. Xie, C. Duan, K. Yan, M. Lin, L. Lou, S. Xia, and J.-C. Krupa, “Preparation and Size Effect On Concentration Quenching Of Nanocrystalline Y_2SiO_5:Eu,” *Chem. Phys. Lett*. 292 (1998), pp. 133-136.

Ziock, K. P., M. T. Burks, W. Craig, L. Fabris, E. L. Hull, and N. W. Madden, “Real-Time Generation of Images With Pixel-by-Pixel Spectra For a Coded Aperture Imager with High Spectral Resolution,” *Nucl. Instr. Meth*. A 505 (2003), pp. 420-424.

Ziock, K. P., W. W. Craig, L. Fabris, R. C. Lanza, S. Gallagher, B. K. P. Horn, and N. W. Madden, “Large Area Imaging Detector for Long-Range, Passive Detection of Fissile Material,” *IEEE Trans. Nucl. Sci*. 51 (2004), pp. 2238-2244.